# DRIED DISTILLERS GRAINS WITH SOLUBLES AS A MULTIFUNCTIONAL FILLER IN WOOD PARTICLEBOARDS

A Thesis
Submitted to the Graduate Faculty
of the
North Dakota State University
of Agriculture and Applied Science

By

David John Sundquist

In Partial Fulfillment of the Requirements
for the Degree of
MASTER OF SCIENCE

Major Program:
Mechanical Engineering

March 2015

Fargo, North Dakota

# North Dakota State University
## Graduate School

**Title**

Dried Distillers Grains with Solubles as a Multifunctional Filler in Wood Particleboards

**By**

David John Sundquist

The Supervisory Committee certifies that this ***disquisition*** complies with North Dakota State University's regulations and meets the accepted standards for the degree of

**MASTER OF SCIENCE**

SUPERVISORY COMMITTEE:

Dr. Dilpreet Bajwa
Chair

Dr. Annie Tangpong

Dr. Chad Ulven

Dr. Sreekala Bajwa

Approved:

4/1/2015
Date

Dr. Alan R. Kallmeyer
Department Chair

# ABSTRACT

Dried Distillers Grains with Solubles (DDGS) has been investigated for its use as a functional filler in wood particleboards bonded with Melamine Urea Formaldehyde. Both the concentration of the DDGS filler – 5, 10, and 15 wt. % – and the particle size of the filler – 125, 300, and 500 µm – has been considered. It was presumed that the additional protein and fats in the lignocellulosic DDGS would increase strength and water resistance of the particleboards. Chemical analysis, thermogravimetric analysis, and differential scanning calorimetry were used to analyze the DDGS filler. A variety of mechanical tests were performed including: flexural, internal bond, hardness, screw withdrawal, linear expansion, and water absorption. The results show that DDGS bonded to the MUF resin. At concentrations of 5 wt. % DDGS with particles of 500 µm produced superior properties compared to the control panel were achieved while the other blends remained equivalent to the control.

# ACKNOWLEDGEMENTS

I would like to especially than the North Dakota Corn Council for providing the funding this research project. Your investment is greatly appreciated. I would also like to thank my Advisor Dr. Dilpreet Bajwa and my committee members — Dr. Annie Tangpong, Dr. Chad Ulven, and Dr. Sreekala Bajwa — for all the time, assistance, and direction regarding this project. I am privileged to work with you.

I would like to also thank Jeanette Ezzo, Darrin Haagenson, Evan Sitz, Lucas Budzien, and Andrew Norris for the assistance that you have provided me throughout my research. Finally, I would like to thank my loving wife Tabitha for your encouragement and support of me.

# TABLE OF CONTENTS

# LIST OF TABLES

# LIST OF FIGURES

# CHAPTER 1 – INTRODUCTION

Wood and wood products are the largest constituent of housing products. Wood components are widely used in furniture as well as structural components. In 2012, over 3.2 billion square feet of wood particleboards in North America were harvested [1]. This chapter introduces a background on particleboards, including the use of alternative lignocellulosic materials as fillers for particleboards and alternative particleboard binders. Useful background information about corn based Dried Distiller Grains with Solubles (DDGS) is also presented.

## 1.1 – Lignocellulosic Product Boards

### 1.1.1 – Wood Composition

Wood can be divided into two general categories of hardwoods and softwoods. Trees belonging to the hardwood category are angiosperms while trees of the softwood family are gymnosperms. Angiosperms produce a seed that is protected and they generally lose their leaves each year. Examples include oak, maple, and balsa. Gymnosperms are cone bearing trees such that the seed is not protected. Examples of these trees include pines, cedars, and firs [2]. Softwoods are preferred as building materials because they are generally less dense and thus easier to cut and use.

Regardless of the category, wood consists of three basic constituents: cellulose, hemicellulose, and lignin. The amount of each of these constituents varies between species of tree. In Table 1, several species of hardwood and softwood compositions are presented.

Table 1 – Compositions of Select Wood Species [3]

| Constituent | Scots Pine | Spruce | Eucalyptus | Silver Birch |
|---|---|---|---|---|
| Cellulose (%) | 40 | 39.5 | 45.0 | 41.0 |
| Hemicellulose | | | | |
| -Glucomannan (%) | 16.0 | 17.2 | 3.1 | 2.3 |
| -Glucuronoxylan (%) | 8.9 | 10.4 | 14.1 | 27.5 |
| - Other Polysaccharides (%) | 3.6 | 3.0 | 2.0 | 2.6 |
| Lignin (%) | 27.7 | 27.5 | 31.3 | 22.0 |
| Total extractives (%) | 3.5 | 2.1 | 2.8 | 30.0 |

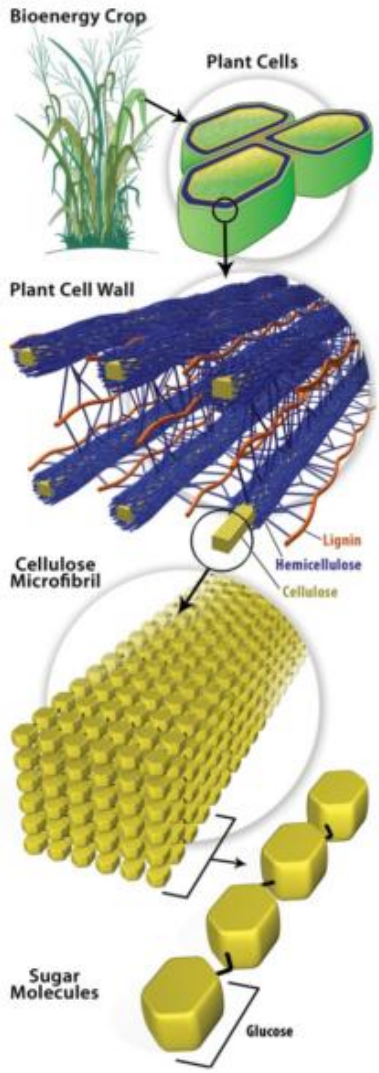


Figure 1 – Arrangement of Cellulose, Hemicellulose, and Lignin [4]

Cellulose is the largest constituent of wood. It is a semi-crystalline polymer comprised of glucose molecules. Cellulose is the base component of the fibrils which are the building blocks of the cell wall. The hemicellulose occurs with cellulose and is comprised of low-molecular weight sugar monomers. The hemicelluloses content varies largely between tree species [2]. Lignin is the second most prevalent wood component. It provides strength to the cell walls and impedes the degradation the cellulose and hemicellulose [5]. Figure 1 shows the arrangement of the different components and depicts their interactions.

### 1.1.2 – Wood Product Boards Classification and Usage

Wood has long been considered a useful engineering material. It possesses a high strength to density ratio which makes it a desired material for construction purposes. Wood is commonly used in joists and beams which exhibit anisotropic properties due to the effect of the grain direction. The waste material from wood products, including chips and sawdust, can be further processed into wood product boards.

Wood product boards are conventionally produced from wood chips and wood flour but can encompass all lignocellulosic materials from plants [6]. These boards are classified into the two broad categories of fiberboards and particleboards. Fiberboards are formed from the fibrous portion of the woody materials. Particleboards are defined by the use of distinct lignocellulosic pieces or particles [6]. Both of these wood product boards require an additional bonding agent to provide the panel's bond strength. Further classifications in each category are designated by particle size and density. Fiberboard examples include hardboards and medium-density fiberboards (MDF). Particleboard examples include plywood, oriented strand board (OSB), and high, medium, and low density particleboards.

Particleboards are widely used as building materials. By reducing the particle size, the properties of these boards behave in an isotropic manner, and the board properties can

be tailored for individual applications. High and Medium density particleboards are used primarily in industrial and commercial purposes. These boards are defined by their density. High density particleboards possess a density greater than 800 kg/m$^3$ while medium density particleboards density range between 800 kg/m$^3$ and 640 kg/m$^3$.

Commercially, they are used in desks, cabinets, tables, and furniture while the construction aspect uses these boards largely for flooring, siding, and insulation [7]. Low density particleboards possess a density less than 640 kg/m$^3$ and are commonly used for door cores. The American National Standards Institute (ANSI) maintain the standards for the particleboards. The physical and mechanical properties regarded by the standard are the modulus of rupture, modulus of elasticity, internal bond, hardness, screw withdrawal, and linear expansion properties. The properties for the high, medium, and low density particleboards are defined in ANSI standard A208.1 2009 update and are provided in Table 2.

Table 2 – Select ANSI 208.1 Standards [8]

| Grade | Physical and Mechanical Properties | | | | |
|---|---|---|---|---|---|
| | Modulus of Rupture (N/mm$^2$) | Modulus of Elasticity (N/mm$^2$) | Internal Bond (N/mm$^2$) | Screw withdrawal (N) | Linear expansion (max %) |
| H- 1 | 14.9 | 2160 | 0.81 | 1600 | n/a |
| M- 1 | 10.0 | 1380 | 0.36 | n/a | 0.40 |
| LD- 1 | 2.8 | 500 | 0.10 | 360 | 0.40 |

### 1.1.3 – Material Usage

Depending upon the board type, the materials used for the production of particleboards come from different sources. Materials for plywood and OSB panels are cut solely for the production of these panels. Materials for particleboards, MDF and hardboards often use lumber mill scrap or recycled materials [2]. The supply of wood for these products has been able to meet the demand since the supply of logged wood in North

America has consistently been less than the net growth of the forests [9]. The future predictions of wood consumption anticipate the use of particleboards and wood products to increase within the next 15 years without surpassing the supply of available materials [10].

## 1.2 – Binders

### 1.2.1 – Common Binders

Currently, synthetic resins are commonly used as the primary bonding agent in particleboards. Three types of resins — phenol formaldehyde (PF), urea formaldehyde (UF), and methylene diphenyl diisocyanate (MDI) — are primarily used in various applications.

PF and MDI resins are commonly used in areas of excessive moisture such as outdoor or bathroom applications [2]. Even though these resins have improved water resistance, their cost is substantially greater than that of UF resins. UF resins are utilized where exposure to moisture is minimal because the cured resin deteriorates in moist conditions. Applications of this binder include interior furniture and other similar products.

These synthetic resins also produce health concerns. Formaldehyde is a known carcinogen and can cause respiratory problems or cancer at low doses. MDI, while less toxic than formaldehyde, also is hazardous to workers and can cause respiratory issues [11]. The California Air Resources Board (CARB) has recently developed standards for formaldehyde emissions, and new resin systems are being developed to meet these standards [2]. The drive to lower emissions has influenced research into alterative binders including natural proteins.

### 1.2.2 – Proteins as Binders

In the past, various protein sources have been used for binders and adhesives including animal protein and vegetable protein. These natural-based adhesives were replaced in the middle of the 1930's with synthetic resins which exhibited superior water resistance [12]. Now renewable binders are again being considered as a replacement for the expensive and hazardous synthetic binders used.

The principles of these binders are inherent to the structure of protein itself. Protein is a polymer chain formed from many different amino acids. The functional groups of the amino acids consist of at least one amine and one carboxylic acid. A peptide is formed when the amino acids amine group reacts with a carboxylic acid group of a different molecule forming a peptide bond.

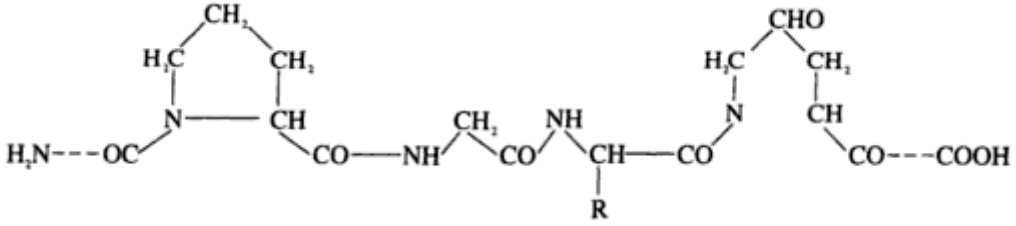


Figure 2 – Peptide Chain Consisting of Three Amino Acid Groups [13]

Protein structure consists of three different phases. The primary structure, shown in Figure 2, represents the strongest cohesive strength of the protein which is the covalent peptide bond between the nitrogen and carboxylic acid's carbon. The secondary structure forms from the hydrogen bonding between the amines hydrogen and the carboxylic acids oxygen creating a three dimensional structure. This structure can form two different phases the α-helix and ß- pleated sheet. Figure 3 depicts the α-helix of the most common corn protein and major component of DDGS Zein. In Figure 3, the amino acid groups contributing to hydrogen bonding are identified.

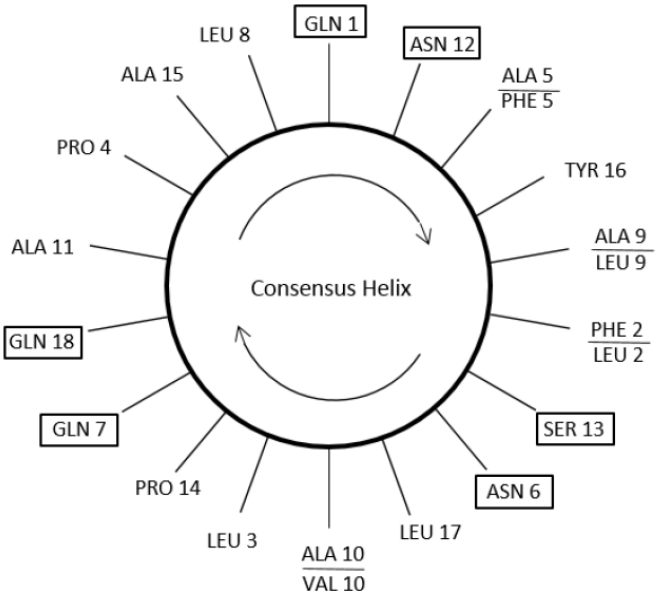


Figure 3 – Zein α – Helix [14]

The tertiary structure is the final structure of the protein molecule. It is the active structure that the entire peptide chain forms. This structure is held together by hydrogen bonding, electrostatic interactions and van der walls interactions.

Proteins need to be denatured before they will effectively act as an adhesive. Denaturing disrupts the secondary and tertiary structure of the protein leaving only the covalent bonding in the primary phase. The most common methods to denature a protein are to subject it to an acid, base, or increased temperature. The denatured proteins are often emulsified [13] which then allows for secondary bonding to occur easily between the individual peptide chains. A common example of a protein-based adhesive used for wood products is soy protein mixed with animal blood, which had been used as a binder until 1973 [12].

## 1.3 – Corn DDGS

Dried distillers grains with solubles have been used as animal feed for roughly the last hundred years [15]. These grains are classified as being the dry residue from cereal grains that are the byproduct from making alcohol or other liquors. During the fermentation process, the starches in the grains are converted into alcohol producing a co-product containing proteins, fats, and fibers. The composition of the distiller grains and the output quantities of alcohol depend upon the initial composition of the grains most importantly the starch concentration.

Table 3 – Composition of Various Cereal Grains [15]

| Cereal Grain | Protein | Oil | Starch | Ash | Total CHO |
|---|---|---|---|---|---|
| Barley | 10.9 | 2.3 | 53.4 | 2.4 | 84.4 |
| Corn | 10.2 | 4.6 | 69.5 | 1.3 | 83.9 |
| Millets (Pearl) | 10.3 | 4.5 | 58.9 | 4.7 | 80.5 |
| Oats | 11.3 | 5.8 | 55.5 | 3.2 | 79.7 |
| Rice | 8.1 | 1.2 | 75.8 | 1.4 | 89.3 |
| Rye | 11.6 | 1.7 | 71.9 | 2 | 84.7 |
| Sorghum | 11 | 3.5 | 65 | 2.6 | 82.9 |
| Triticale | 11.9 | 1.8 | 71.9 | 1.8 | 84.5 |
| Wheat | 12.2 | 1.9 | 68.5 | 1.7 | 84.2 |

In recent years, corn has widely been used to produce ethanol used as a replacement and additive of gasoline. As can be seen from Table 3, corn does not have the highest starch content of the various cereal grains, but it is the most abundant grain in the US [16]. Roughly for every bushel of corn processed, 8.16 kg of DDGS and 11 liters of ethanol are produced.

The amount of DDGS produced is steadily increasing as is the production of ethanol in the US. Figure 4 shows the increasing amounts of DDGS being produced from corn ethanol plants since 1990 with 35 million metric tons produced in 2012.

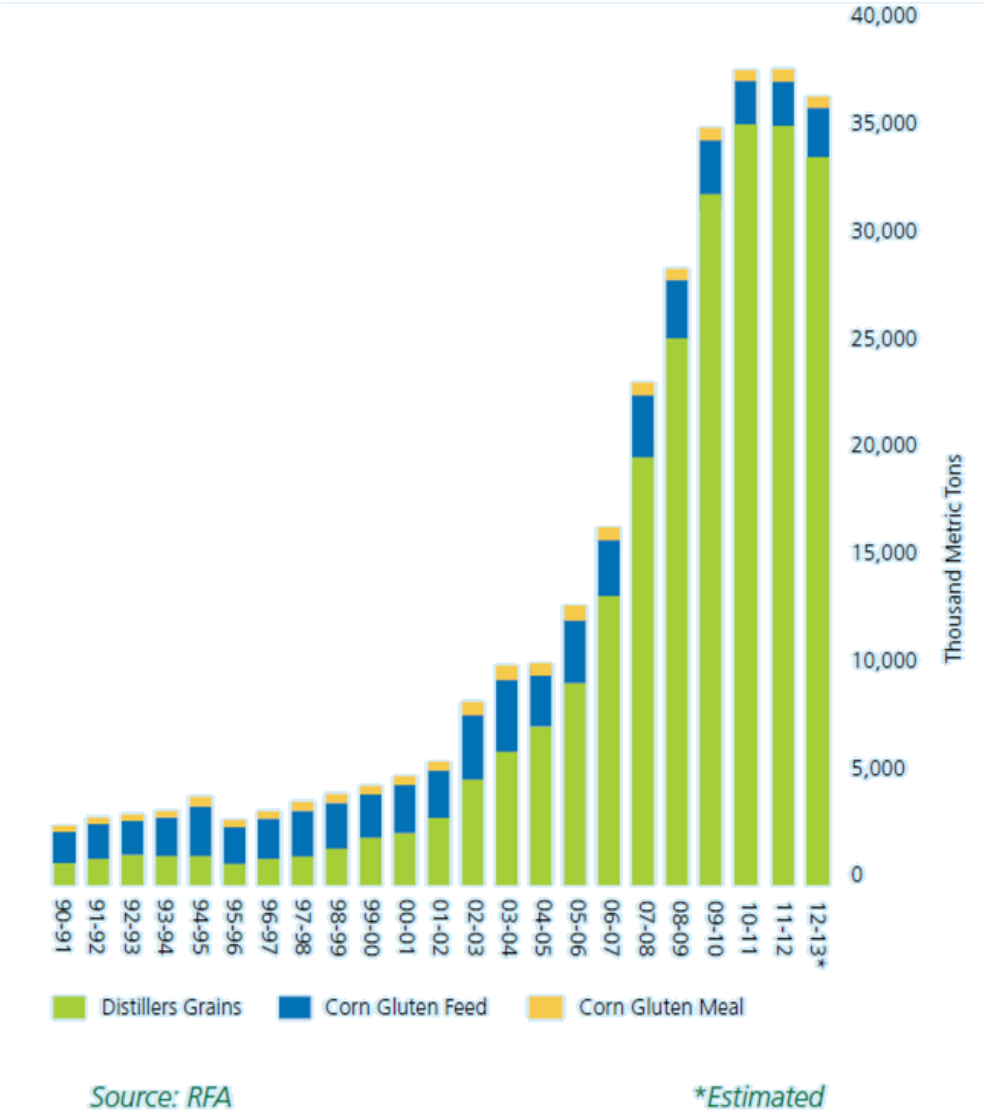


Figure 4 – DDGS Production in US since 1990 [17]

Currently, the majority of DDGS is utilized as feed stock. With the increasing production of DDGS, further markets have been explored so that the value of DDGS will not diminish. These markets include fish feed, human consumption, and industrial uses [15].

### 1.3.1 – Corn Kernel Structure

The corn kernel consists of three major components: the endosperm, hull, and germ which are depicted in Figure 5. Each component has various concentrations of protein, fat, starch, and cellulose.

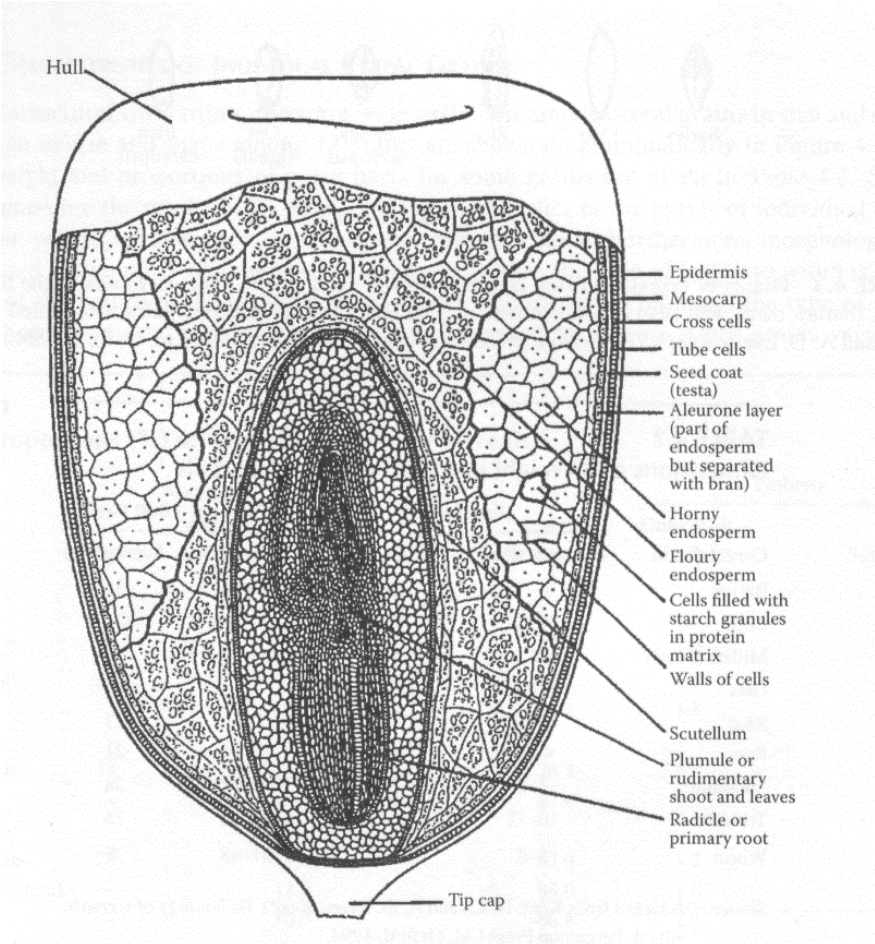


Figure 5 – Corn Kernel [15]

The majority of the kernel is endosperm which contains high concentrations of protein and starch. The germ is comprised majorly of lipids and proteins while cellulose and hemi-cellulose fibers comprise the hull of the kernel. Lignin is found throughout the kernel as it acts as a binding agent.

### 1.3.2 – DDGS as a Bi-Product of Ethanol

There are two different types of processing methods used in the production ethanol: dry and wet. These processes only differ in the first step in which the kernel is ground. A general overview of the ethanol process is illustrated in Figure 6.

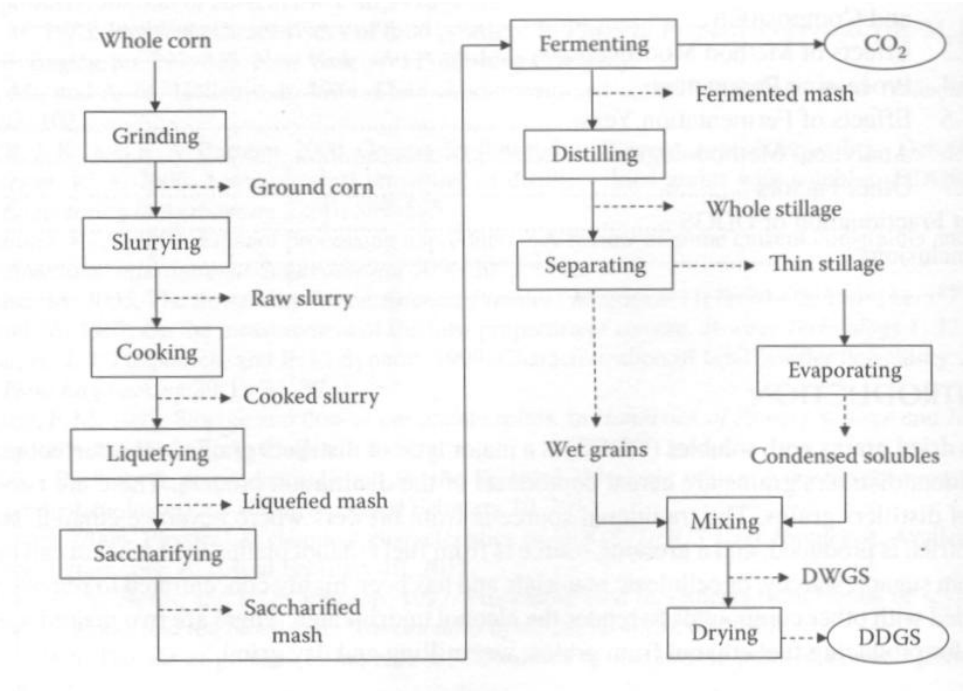


Figure 6 – Dry Grind Ethanol Process Diagram [15]

Corn kernels are initially ground in order to expose the starch containing endosperm. The ground corn is then cooked and fermented. During the fermentation process, starch is converted into ethanol and carbon dioxide.

$$C_6H_{12}O_6 \rightarrow 2C_6H_5OH + 2CO_2(g) \qquad \text{Equation 1}$$

After ethanol is distilled from the slurry, the remaining proteins, fats, and cellulosic materials are dried to form DDGS. The high protein, fat, and fiber contents in DDGS make this material a suitable animal feed but also a promising material as an alternative cellulosic material for particleboards.

# CHAPTER 2 – BACKGROUND AND LITERATURE REVIEW

This chapter provides information and discusses research involving particleboard production, composition, and different binders. Research regarding DDGS is also discussed, and its properties are presented.

## 2.1 – Particleboard Research

Due to the large demand for wood products, many improvements and modifications of these products can occur. It is theorized that the current wood usage comprises only four percent of the theoretical amount of products that can be formed from lignocellulosic materials [7]. Current research into the improvement of lignocellulosic boards is focused on how the addition of alternative lignocellulosic materials and the processing affect the mechanical properties.

### 2.1.1 – Processing Effects

With the implementation of alternative lignocellulosic materials, several processing parameters have been identified that affect the mechanical properties. These parameters include the press time, press temperature, particle drying, and particle size.

#### 2.1.1.1 – Press Time and Temperature

Pressing time affects the strength of the binders. A shortened press time results in an insufficiently cured binder due the limited heat penetration [18] thus lowering the internal bond strength of the board. An increased press time has also been shown to negatively affect the tensile strength and bending strength of the synthetic resin free, or binderless, boards due to the degradation of the strength bearing fibers [19].

The press temperature also affects the properties of the panels. It has been shown that the various lignocellulosic binders' properties are temperature dependent and

characteristic of each binder [20]. An increase in press temperature has been shown to improve the water absorption properties of binderless boards [21] and can reduce required the press time. In addition to the press temperature, steam pressing will improve the mechanical properties of binderless boards when compared simply to dry hot pressing [22]. The addition of moisture increases the heat transfer and the hydrogen bonding between proteins [19].

#### 2.1.1.2 – Particle Drying

Particle drying is important as it improves the panels' mechanical properties when compared to green particles [20]. Some moisture is useful to the curing process as it increases as is observed in the addition of steam to the hot pressing. The drying temperature is also an important processing parameter. Increasing the drying temperature increases the degradation of the hemicellulose content [23]. The degradation of hemicellulose decreases the degree of polymerization that can be achieved, thus reducing the mechanical properties of the boards [24].

#### 2.1.1.3 – Particle Size

The reduction of particle size largely influences the tensile strength, toughness, and stiffness [25, 26]. This effect is caused by the increase of the particle's surface area improving the load transfer between the matrix and the fiber [25 – 27].
The increase in surface area also increases the adhesion of the particles. The increase in the surface area creates more exposed functional groups on protein, lignin, and hemicellulose this improving the bonding in the boards [21]. The reduction of particle size with differing lignocellulosic fillers produces different properties because of the variations of chemical composition [28].

Well-dispersed particles also improve the adhesion of alternative binders. Liquid dispersions of proteins have been shown to exhibit better properties than a dry mixture of the same particle size [20].

### 2.1.2 – Alternative Resins

Common binders used in the manufacturing of particleboards are urea-formaldehyde (UF), melamine formaldehyde (MF), phenol formaldehyde, or isocyanate based resins [7]. The cost and the health hazards of these resins create the fundamental drive to find renewable alternative resins. In the past, natural protein based resins have been used to produce lignocellulosic materials. Current research shows that plant proteins can be an effective supplement or replacement to the petroleum-based resins.

Soy-protein-based resins have been commonly used as a natural resin for particleboards in the past [12] and are a common starting point for current research. Besides soy protein, wheat gluten and cotton seed protein can be used as an effective alternative in particleboards [20, 29].

Corn proteins are commonly used as an extension in resins. Corn protein extract and corn starch based binders have exhibited superior properties when compared with commercially available alternatives [30 – 32]. Corn meal extended PF resins exhibit properties suitable for plywood and fiberboards [33, 34].

Pure corn-based binders have also been developed. Zein has been used as the sole binder in biopolymer composites [35]. Corn gluten meal has exhibited thermoplastic properties due to strong protein interactions, which have been utilized to produce wood based composites [36].

Other forms of protein have also been investigated including blood meal and peanut flour. The blood meal and peanut-based binders meet the requirement for exterior and

interior MDF boards, respectively [37]. The effectiveness of these alternative resins are largely dependent upon the chemical composition of the plant which affects the adhesion in wood based products [20, 38].

### 2.1.3 – Binderless Boards

Research has also been performed to replace the petroleum-based resin completely. Starch has been used to create a binder for medium density fiberboards [39]. Lignocellulosic materials have also been used to produce binderless boards. Sugi heart and sapwood have also been used to produce binderless boards in Japan [32]. Kenaf core-powder-based binderless boards are currently being developed with further research focused on improving the water absorption properties [19, 21].

Bagasse, the remnant of sugarcane processing, is one of the most promising lignocellulosic materials [22]. The bagasse-based binderless particleboards perform similarly to their resin based counterparts [40]. The various attempts at creating binderless boards show the potential of using purely the functional chemical components of plants as binders, but future research needs to be performed to improve the water absorption of the binderless boards.

### 2.1.4 – Alternative Biomass Fillers

Various types of lignocellulosic materials can be combined with wood for a mixture of new properties [41]. Post-processed lignocellulosic materials are in abundance and have great potential to be supplemented into particleboards. Bagasse and hemp have been supplemented up to 50 wt. % and either outperform the reference wood particleboards or meet the standard properties [42]. Canola particles also exhibit adequate properties up to 30 wt. % loading [42]. DDGS is an additional lignocellulosic waste material that may have potential for use in particleboards.

## 2.2 – DDGS

This section considers the properties of the DDGS and discusses relevant research involving DDGS as a filler for composites.

### 2.2.1 – Properties and Composition

The properties of DDGS vary due to how it is processed and the growing conditions of the harvested year [15]. Therefore, substantial research has been conducted to characterize the properties of DDGS. The properties determined are similar to other dry feed stock [43] and are presented in Table 4.

Table 4 – Typical Properties of DDGS [15]

| Property | Range |
|---|---|
| Geometric Mean Diameter ($d_{gw}$, mm) | 0.21 - 1.38<br>0.68 - 1.862<br>0.434 - 0.949<br>0.073 - 1.217<br>0.256 - 1.087<br>0.61 - 2.13 |
| Geometric Standard Deviation ($S_{gw}$, mm) | 0.20 - 0.55<br>0.418 - 1.494<br>0.26<br>0.28<br>1.56 - 2.75 |
| Bulk Density (BDA, kg/m$^3$) | 490 - 600<br>414.37 - 577.78<br>389.3 - 501.5<br>365.22 - 504.58 |
| Moisture Content (%, db) | 13.2 - 21.2 |
| Thermal conductivity (W/(m˚C) | 0.06 - 0.08 |

The particle size of the DDGS is an important classification of the grains. The particle sizes vary greatly depending upon the processing but the distribution generally falls between 0.1 and 4 mm with the majority of the particles approximately 0.5 mm in diameter [44].

The structure of how the protein, fats, and carbohydrates arrange themselves in the individual particles affects how the material can bond with itself.

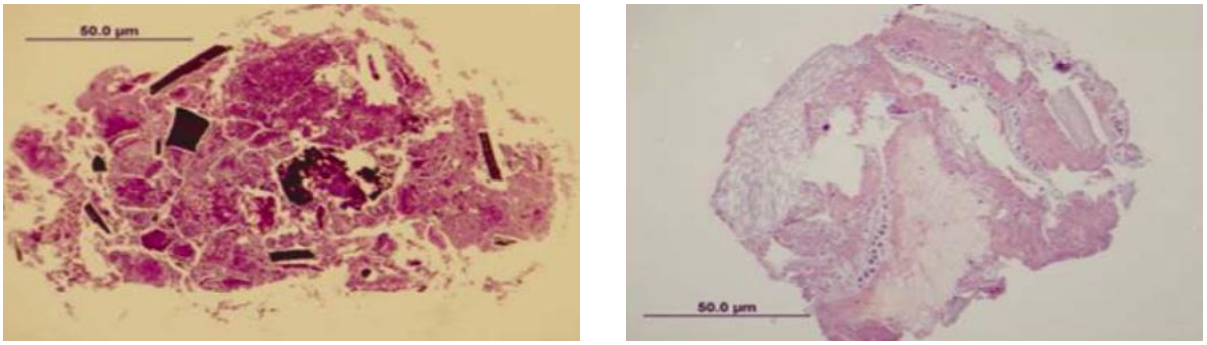


Figure 7 – Stained Cross Section of DDGS Particles [45]

In Figure 7, cellulose is darkest followed by protein and fat. This shows that the surface of the DDGS particles are largely composed of the protein and fats while the cellulose contributes to the internal structure of the particle. The presence of the surface fats and proteins increase the self-adhesion and bendability of DDGS [45].

### 2.2.2 – DDGS Research

As previously discussed, corn protein shows promise as an alternative resin. Minimal research has been conducted regarding DDGS filled composites. As a filler for thermoplastics, DDGS thermoplastics generally exhibit a decrease in mechanical properties [28]. Superior properties can be achieved by incorporating a coupling agent [46]. DDGS incorporation into thermosets shows promise. It has been shown that DDGS can be incorporated into phenolic resin at 25% loading while maintaining mechanical properties [47]. Further testing showed that an increase to 50% with only a slight reduction of properties [48]. DDGS has also been incorporated into resin glues [49]. In all cases, the predominate downfall of the filler is an increased water absorption [47 –49].

While more research needs to be completed, DDGS shows promise as a filler for both thermosets and thermoplastics. Moreover, it has great potential to be incorporated into lignocellulosic boards as a supplemental material.

# CHAPTER 3 – OBJECTIVES

The objective of this research is to understand if the addition of DDGS particles in the wood particleboards will improve the mechanical properties of low-density particleboards. In order to fully investigate the effects of the DDGS filler, different concentrations and particle sizes will be investigated. This study will also identify the chemical composition of DDGS.

Through this research, the following hypotheses will be investigated.

H1: The protein of the DDGS can be decoupled via heat and subsequently fully bonded to the MUF resin.

H2: The decrease of particle size of the DDGS filler will improve the mechanical properties.

H3: Higher concentrations of DDGS will not significantly influence the mechanical performance of the particleboards.

H4: The residual fat in DDGS will decrease the linear expansion and water absorption of the particleboards.

A successful study will prove or disprove each of the hypothesis and characterize the DDGS filler.

# CHAPTER 4 – MATERIALS AND METHODS

In this chapter, the materials used in this experiment are presented. The method used to produce the panels are presented as well as the various tests and analytical methods used.

## 4.1 – Materials

Pine wood flour was acquired from American Wood Fibers (Wausau, WI). A 2020-grade fiber was used in this experiment. The particle distribution of this grade of pure wood fiber is shown in Table 5.

Table 5 – Particle Distribution for 2020 Grade Wood Fiber

| U.S. Standard Sieve and Micron Equivalent | Content |
|---|---|
| 10 Mesh (2000 µm) | < 0.36 % |
| 20 Mesh (850 µm) | 0 – 5 % |
| 40 Mesh (425 µm) | 40 – 80 % |
| 60 Mesh (250 µm) | 15 – 55 % |
| Pan | < 10 % |

The resin used was LEAF™ 778G80 MUF resin from Georgia- Pacific Chemicals (Eugene, OR). This resin meets all proposed Carb2 emissions standards and has a solids content of 65%. The paraffin wax emulsion AW 50 was acquired from A&W Products Inc. (Bishop, GA) and used in this experiment. The DDGS was acquired from a BlueFlint Ethanol plant located near Underwood, North Dakota. The unprocessed DDGS had an average particle size of 500 µm and a particle distribution shown in Figure 8.

The particle size of the DDGS was reduced via a Retsch Rotor Beater Mill 300 (Newtown, PA), portrayed in Figure 9. Some of the unprocessed DDGS was ground and classified to achieve an average particle size of 300 µm and 125 µm.

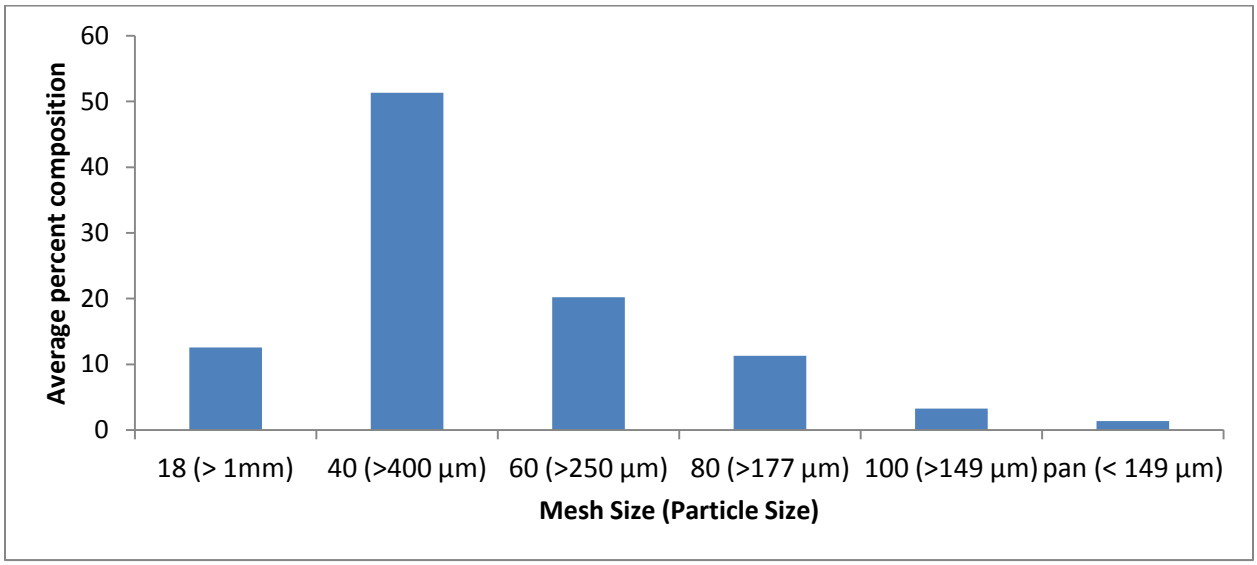


Figure 8 – Average Particle Distribution for Unprocessed DDGS


Figure 9 – Retsch Rotor Beater Mill SR 300

The DDGS and wood fiber were dried in ambient conditions, based upon the Forest Products Laboratory's recommendation [2], to between 4 and 6 percent moisture.

## 4.2 – Panel Processing

The wax and resin were added to the conditioned DDGS and wood fiber through a standard paint sprayer. While the wax and resin were being sprayed, the DDGS and wood fiber were continually agitated in a cement mixer (Figure 10) in order to achieve a uniform distribution.

Figure 10 – Cement Mixer used to Agitate DDGS and Wood Fiber

After the wax and resin were sprayed into the agitated mixture, the fiber was laid into an internally produced mold for pressing (Figure 11). The fiber was weighed in order to achieve a target density of 640 kg/m$^3$ for the panels. The fibers were pressed and heated via a Carver Hot Press Model 4122 (Wabash, IN) shown in Figure 12. The processing conditions for the press are provided in Table 6.

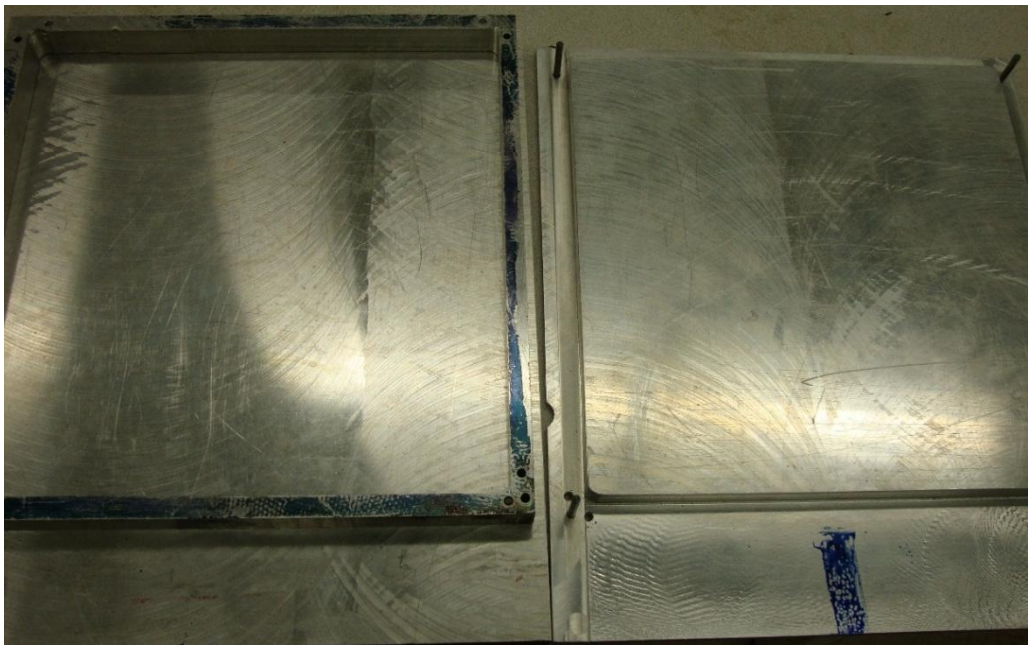

Figure 11 – Mold for Panel Pressing


Figure 12 – Carver Press Model 4122

Table 6 – Process Conditions for Panel Pressing

| | |
|---|---|
| Upper Platen Temperature | 200 ˚C |
| Lower Platen Temperature | 200 ˚C |
| Press Time | 10 minutes |
| Pressure | 10 Metric Tons |
| Time to Max Pressure | < 1 minute |

After it was pressed, the panel was removed from the mold and allowed to cool for a minimum of 24 hours before further handling.

## 4.3 – Design of Experiment

A full factorial design of two factors and three levels or a $3^2$ factorial design was developed. The two factors investigated were the DDGS particle size and DDGS filler concentration tested at three different levels. The particle sizes of DDGS were 500, 300, and 125 µm, and the loading concentrations were 5, 10, and 15 wt. % DDGS fiber. In addition to the factorial design, a control sample was produced with no DDGS filler. In total, 10 different blends were studied in this experiment which are shown in Table 7. In each case, the resin wt. % and wax wt. % content remained constant at 10 wt. %, respectively. Four 305 x 305 mm panels were produced for each blend, and all samples for testing were cut from them.

Table 7 – Design of Experiment and Number of Panels Produced

| DDGS Concentration \ Particle Size | Unprocessed (mean 500 µm) | 300 µm | 125 µm |
|---|---|---|---|
| 5 wt. % | 4 | 4 | 4 |
| 10 wt. % | 4 | 4 | 4 |
| 15 wt. % | 4 | 4 | 4 |
| 0 wt. % (Control Sample) | 4 | | |

Each sample was produced with a target density of less than 640 kg/m$^3$ thus meeting the criterion of a low-density particleboard.

## 4.4 – Analytical Analysis

Several tests were performed to characterize the DDGS filler and to understand the interaction between the MUF resin and the DDGS filler. To characterize the DDGS filler,

chemical analysis and thermogravimetric analysis were performed for each DDGS particle size and also the components of DDGS including defatted DDGS, Zein protein, and corn fiber consisting of the cellulosic components from DDGS. The Zein used was F4000 grade from FLO Chemical Corporation (Ashburnham, MA). The corn fiber was extracted from DDGS at Mississippi State University in Starksville, MS. Differential scanning calorimetry and fourier transform infrared spectroscopy were used to determine the bonding of the MUF resin to the DDGS.

### 4.4.1 – Chemical Analysis

Chemical analysis was performed on the DDGS particles, Zein protein, and corn fiber by the nutrition lab in the Animal and Range Science Department at North Dakota State University (NDSU) in Fargo, ND. All tests followed the Association of Analytical Community's (AOAC) Methods. The analysis was performed with 3 replications and using alfalfa as a control specimen. The data collected included dry matter, ash, crude protein, nitrogen, neutral detergent fiber, acid detergent fiber, and crude fat. The neutral detergent fiber and acid detergent fiber consist of the cellulose, hemicellulose, and lignin. The acid detergent fiber contains the cellulose and lignin. Thus the hemicellulose can be found from the difference between the neutral detergent fiber and the acid detergent fiber as shown below.

$$\%Hemicellulose = \%NDF - \%ADF \qquad \text{Equation 2}$$

### 4.4.2 – Thermogravimetric Analysis

Thermogravimetric analysis (TGA) was used to determine the degradation temperature of the DDGS. Each component was run to determine its effect of the overall degradation curve of DDGS. From the results, an operating temperature for the press was determined. The analysis was performed at NDSU's Center for Nanoscale Science and

Engineering Center with a TA Q500 TGA (New Castle, DE). The temperature was ramped from 25 ˚C to 400 ˚C at 10 ˚C/min. Air was used as the flow gas at 20 ml/min.

### 4.4.3 – Differential Scanning Calorimetry

Differential scanning calorimetry was performed at NDSU's Center for Nanoscale Science and Engineering Center using a TA Q1000 DSC (New Castle, DE). A heat, cool, heat cycle was used to cure the MUF/DDGS mixture and then check its crosslinking. The temperature ranged from 25 ˚C to 200 ˚C at 10 ˚C/min. The chamber was purged with nitrogen gas at rate of 50 ml/min. Seven different combinations of resin and DDGS were tested. A 1.5/1 wt. ratio of DDGS to resin was tested to mimic the 15 wt. % loading case, and a 1/2 wt. ratio was tested to simulate the 5 wt. % loading case. All samples were run with all three particle sizes, and a pure MUF resin and Zein protein were also analyzed.

### 4.4.4 – Fourier Transform Infrared Spectroscopy

Fourier Transform Infrared Spectroscopy (FTIR) was performed by the Agricultural and Bio-systems Engineering department at NDSU. The testing was performed on a Thermo Scientific Nicolet 6700 FTIR spectrometer with a germanium crystal. Three samples were tested including pure MUF resin, DDGS and MUF resin, and Zein protein and MUF resin. The purpose of the analysis was to determine the change of the functionality of MUF resin with the addition of the DDGS and protein.

## 4.5 – Mechanical and Physical Testing

Several tests were performed to evaluate the change of physical properties of the samples. These tests included density, linear expansion, and water absorption. Mechanical properties of the boards were determined from the static bending, internal bond, screw

withdrawal, and hardness tests. Samples for these tests were cut from the four boards in the pattern provided in Figure 13 which was adapted from ASTM D1037.

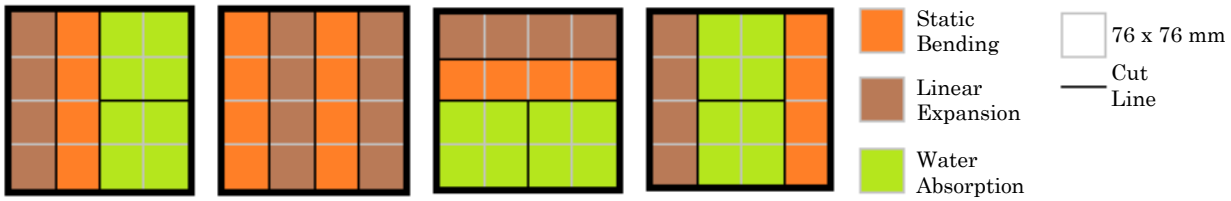


Figure 13 – Sample Selection Pattern for Testing

The hardness, internal bond, and screw withdrawal samples were cut from the static bending and linear expansion samples post testing.

### 4.5.1 – Density Measurement

The density was calculated by measuring the mass of the entire board (m) and the volume of the panel. The mass was measured to ±0.1 gram. The volume was calculated from the average of 3 length measurements (L), 3 width measurements (W), and 4 thickness measurements (T). These measurements were measured to ±0.01 mm. The density was then calculated based on the following equation in accordance with ASTM D2395.

$$Density = \frac{m}{LWT} \qquad \text{Equation 3}$$

### 4.5.2 – Linear Expansion Testing

Linear expansion tests measure how a material expands in the presence of humidity. Low expansion is desired because it indicates a material resilient to humidity. Thus preventing dimensions to fluctuate with climate variability.

Linear expansion tests were performed using a Binder Humidity Chamber model KBF 115 – UL. Samples were in the dry condition at 50% humidity and had dimensions of 76 mm x 305 mm. The samples were exposed to 80% humidity at 20 ± 3 ˚C for 30 hours in

to reach their equilibrium state. The sample lengths were then measured from the center of the board, and the linear expansion was calculated.

$$\%\ Change\ of\ Length = \frac{L_f - L_i}{L_i} \qquad \text{Equation 4}$$

Where $L_i$ is the initial length at 50% humidity and $L_f$ is the length at 80% humidity.

### 4.5.3 – Water Absorption Testing

Water absorption tests measure the resilience of a particle board to absorb water. In this test, an increase weight and volume change signifies that the particleboard absorbed water. The minimum change of weight and volume shows superior water resilience and is a desirable attribute of particleboards.

Dry 152 mm x 152 mm square samples were submersed horizontally in tap water according to ASTM D1037. The tank was maintained at 20 ± 1 ˚C. Testing followed the 2+22 method meaning that the samples were removed from the bath at 2 hrs. The specimens were then allowed to drain for 10 minutes and their length, width, thickness, and weight were measured. After a total of 24 submersed hours, they were removed and measured again. The percent change of mass and volume were calculated based upon their dry condition by the following equations.

$$\%\ Change\ Mass = \frac{(M_f - M_i)}{M_i} \qquad \text{Equation 5}$$

Where $M_f$ if the mass after submersion and $M_i$ is the mass of the dry condition.

$$\%\ Change\ Volume = \frac{V_f - V_i}{V_i} \qquad \text{Equation 6}$$

Where $V_f$ is the final volume, $V_i$ is the initial or dry volume, and the volume is calculated by

$$V = LWT \qquad \text{Equation 7}$$

Where L is the length, W is the width, and T is the average thickness of four thickness measurements.

### 4.5.4 – Static Bending Testing

Three-point static bend testing measures the stiffness of a sample. A high stiffness is desirable to reduce the deformation of particleboard products used in load bearing conditions. The fixture and loading conditions are presented in Figure 14.

Figure 14 – Three Point Flexural Test

Three-point static bend testing was performed on an Instron load frame Model 5567 in accordance with ASTM D1037. The sample geometry was 76 mm wide and 305 mm long with a span of 200 mm. The crosshead speed for testing was calculated by the equation below.

$$N = \frac{33.3}{t} \qquad \text{Equation 8}$$

Where t is the thickness of the sample.

The modulus of rupture ($R_b$) and modulus of elasticity (E) were calculated based from Equation 4 and Equation 5, respectively.

$$R_b = 300\frac{P_{max}}{w\,t^2} \qquad \text{Equation 9}$$

$$E = \frac{2e6\,\Delta P}{wt^3\,\Delta l} \qquad \text{Equation 10}$$

Where $w$ is the width of the sample, $t$ is the thickness, $P_{max}$ is the maximum load in newtons, and $\Delta P/\Delta l$ is the slope of the linear portion of the deflection curve.

### 4.5.5 – Internal Bond Testing

Internal bond testing measures the cohesive strength of a panel. High internal bond strength signifies that the samples are well bonded. Square samples were cut to a length and width of 51 mm and glued to the loading blocks. The glue used was a hot melt adhesive provided from Primeboard Masonite in Wahpeton North Dakota. The loading blocks were heated on a hot plate and glue applied to the surface. The sample was placed on the melted glue and the blocks were allowed to cool for a minimum of one hour. Then the process was repeated for the second surface.

Testing was performed on an Instron model 5567 load frame at a rate of 1 mm/min. Adhesive failures between the glue and loading block were discarded and not included in the analysis. The fixture and loading blocks can be observed in Figure 15.

Figure 15 – Internal Bond Test Fixture and Loading Blocks

The maximum stress was calculated by

$$\sigma_{max} = \frac{P_{max}}{wl} \qquad \text{Equation 11}$$

Where $w$ is the width of the sample, $l$ is the length of the sample, and $P_{max}$ is the maximum load in newtons.

### 4.5.6 – Screw Withdrawal Testing

Screw withdrawal tests measure how well a panel will support a fastener. A high screw withdrawal force indicates a material can easily support a screw. Screw withdrawal tests were performed on square samples 76 mm wide of manufactured thickness. The screw used was a Number 10 type AB with pitch of 16 threads per inch in accordance with ASTM D1037. All samples were predrilled in the face using a 1/4 inch drill bit.

Samples were tested in the dry condition on the aforementioned Instron Universal Load Frame within 15 minutes of application of the screw. The strain rate used was 15 mm/min, and the sample was housed in internally produced fixtures as shown in Figure 16.

Figure 16 – Screw Withdrawal Test

### 4.5.7 – Hardness Testing

Hardness tests measure the ability of a substrate to resist deformation. A large hardness is desirable which would prevent a particleboard based material from denting under normal circumstances. Hardness testing was performed on square samples 76 mm wide by twice the manufactured thickness. This thickness was achieved by gluing two

samples together using Weldwood Contact Cement following the ASTM standard. The janka ball method was used to test hardness with a 9.5 mm diameter 'ball' shown in Figure 17.

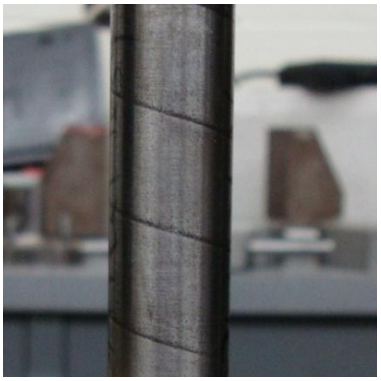

Figure 17 – Hardness Testing Apparatus

Testing was performed on the Instron Load Frame. The strain rate used was 6 mm/min in accordance with ASTM D1037. The test was stopped when the 'ball' penetrated 4.75 mm, and the maximum force was recorded as the hardness value.

## 4.6 – Statistical Methods

In this research, statistical methods were used to analyze the data in order to observe the interaction of the DDGS particle size and concentration. All statistical analyses were performed in the statistical software program Minitab. Three main tools were used: the boxplot, two-way t test, and analysis of variance (ANOVA).

### 4.6.1 – Boxplots

Boxplots are useful tools which depict a graphical representation of the data. A description of a boxplot is provided in Figure 18.

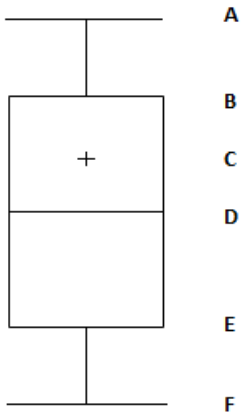


Figure 18 – Boxplot Diagram

Where A is the maximum value, B is the 3rd Quartile, C is the mean of the data set, D is the median of the data set, E is the 1st Quartile, and F is the lowest value.

The 1st quartile is the value at which 25% of the data is smaller and 75% is larger. The 3rd quartile is the value at which 75% of the data set is smaller and 25% is larger than the quartile. The ordered observation of the quartile in an ascending arrangement of the data is calculated by the following equation.

$$q_i = \frac{i(n+1)}{4} \qquad \text{Equation 12}$$

Where n is the number of data points, and i represents the quartile of interest. The quartile is the data point that is in the position of the ordered observation in the ascending arrangement of data values.

### 4.6.2 – Student – T Test

The two-way t test or test between two means is a useful tool to test whether the means of two independent samples are statistically equivalent. For this test, it is assumed that the population variances are equal. With this assumption, the t test can be reduced to the following equation.

$$t = \frac{(\overline{X_1} - \overline{X_2}) - (\mu_1 - \mu_2)}{\sqrt{(S_p^2)\left(\frac{1}{n_1} + \frac{1}{n_2}\right)}} \quad \text{Equation 13}$$

Where $\overline{X_i}$ is the sample mean, $\mu_i$ is the population mean, n is the number of samples. $S_p$ is defined by

$$S_P^2 = \frac{(n_1 - 1)S_1^2 + (n_2 - 1)S_2^2}{(n_1 - 1) + (n_2 - 1)} \quad \text{Equation 14}$$

Where S is the sample standard deviation. The degrees of freedom for this test is defined by

$$df = n_1 + n_2 - 2 \quad \text{Equation 15}$$

Once the t value is obtained, the calculated probability can be determined using a student t table. For this work, a confidence level of 95% is assumed. Thus, if the calculated probability is greater than or equal to 0.05, the null hypothesis of the equivalent sample means cannot be rejected. If the calculated probability is less than 0.05, the null hypothesis is rejected, meaning the two sample means are statistically different.

### 4.6.3 – ANOVA of a Factorial Design of Experiment

ANOVA is a useful method to compute experimental error within a variable or between different variables. This method fits a model and shows the significance of the effect a variable has on the model at a given confidence. For this analysis, a confidence interval of 95% was used. This signifies that 95% of the data include the true population mean and sample means.

The model variation can be expressed as main effects and interaction effects. The main effects represent the interaction among a particular factor while the interactions are the effects between factors. The variation of the main effects for a two-factor design comes from Factor A and B [50]. The variation for Factor A (SSA) can be calculated by

$$SSA = cn' \sum_{i=1}^{r} (\bar{X}_i - \bar{\bar{X}})^2 \quad \text{Equation 16}$$

Where c is the number of levels of Factor B, r is the number of levels of Factor A, n' is the number of replication, and where $\bar{X}_i$ and $\bar{\bar{X}}$ are defined below.

$$\bar{X}_i = \frac{\sum_{j=1}^{c}\sum_{k=1}^{n'} X_{ijk}}{cn'} \quad \text{Equation 17}$$

When i ranges from 1 to r and $X_{ijk}$ is the k$^{th}$ observation of Factor A or B.

$$\bar{\bar{X}} = \frac{\sum_{i=1}^{r}\sum_{j=1}^{c}\sum_{k=1}^{n'} X_{ijk}}{rcn'} \quad \text{Equation 18}$$

The variation for Factor B (SSB) is defined by

$$SSB = rn' \sum_{j=1}^{c}(\bar{X}_j - \bar{\bar{X}})^2 \quad \text{Equation 19}$$

Where $\bar{X}_j$ is defined by

$$\bar{X}_j = \frac{\sum_{i=1}^{r}\sum_{k=1}^{n'} X_{ijk}}{rn'} \quad \text{Equation 20}$$

The interaction effect of Factors A and B (SSAB) is defined below.

$$SSAB = n' \sum_{i=1}^{r}\sum_{j=1}^{c}(X_{ij} - \bar{X}_i - \bar{X}_j + \bar{\bar{X}})^2 \quad \text{Equation 21}$$

Where $X_{ij}$ is defined by

$$X_{ij} = \sum_{k=1}^{n'} \frac{X_{ijk}}{n'} \quad \text{Equation 22}$$

The sum of squares error (SSE) is defined below.

$$SSE = \sum_{i=1}^{r}\sum_{j=1}^{c}\sum_{k=1}^{n'}(X_{ijk} - \bar{X}_{ij})^2 \quad \text{Equation 23}$$

The mean squared values are calculated by dividing the sum of the square values by the degree of freedom as shown below.

$$MSA = \frac{SSA}{r-1} \quad \text{Equation 24}$$

$$MSB = \frac{SSB}{c-1} \quad \text{Equation 25}$$

$$MSAB = \frac{SSAB}{(r-1)(c-1)} \quad \text{Equation 26}$$

$$MSE = \frac{SSE}{rc(n'-1)} \quad \text{Equation 27}$$

The F test then can be performed to test if the variance is within the confidence interval. The main effect from Factor A is calculated in the equation below.

$$F = \frac{MSA}{MSE} < F_\alpha \qquad \text{Equation 28}$$

Where $F_\alpha$ is determined from any accepted statistical F distribution table using the degrees of freedom used to calculate MSA and MSE respectively with α = 0.05 which corresponds to the confidence interval of 95%.

Likewise, the equation for the main effect from Factor B is below.

$$F = \frac{MSB}{MSE} < F_\alpha \qquad \text{Equation 29}$$

Where $F_\alpha$ is determined from the α = 0.05 F table using the degrees of freedom from MSB and MSE respectively.

The interaction effect can then be determined by

$$F = \frac{MSAB}{MSE} < F_\alpha \qquad \text{Equation 30}$$

Where $F_\alpha$ can be obtained from F table with α = 0.05 using the degrees of freedom from MSAB and MSE respectively. If $F > F_\alpha$ then the main effect or interaction effect is not significant at a 95% confidence level.

# CHAPTER 5 – RESULTS AND DISCUSSION

This chapter presents the experimental results from this study. The tests are divided into two sections: analytical analysis and mechanical testing.

## 5.1 – Analytical Analysis

This section contains the results from the chemical analysis, TGA, and DSC.

### 5.1.1 – Chemical Analysis

Chemical analysis was used to determine the amount of constituents in DDGS. In addition to the DDGS, individual components were analyzed. The results from these tests are shown in Table 8.

Table 8 – Chemical Analysis

| Component | Ash (%) | Crude Protein (%) | Nitrogen (%) | NDF (%) | ADF (%) | Crude Fat (%) |
|---|---|---|---|---|---|---|
| DDGS, 125 | 4.72 | 31.29 | 5.01 | 39.18 | 11.64 | 8.57 |
| DDGS, 300 | 4.70 | 30.08 | 4.81 | 36.95 | 10.26 | 7.83 |
| DDGS, 500 | 4.81 | 30.39 | 4.86 | 41.39 | 12.81 | 7.29 |
| DDGS, 500 (defatted) | 5.31 | 33.49 | 5.36 | 41.33 | 12.01 | 0.00 |
| Corn Fiber | 1.66 | 6.68 | 1.07 | 66.18 | 17.78 | 0.83 |
| Zein F4000 | 1.34 | 87.87 | 14.06 | 0.00 | 0.10 | 0.94 |

From this analysis, several observations can be made. First, the DDGS constituents were similar to other DDGS produced in the Midwest [15]. Secondly, the percent of protein, NDF, ADF, and fat did not vary significantly among the different particle sizes. This shows that the processing did not significantly alter the components of DDGS. The corn fiber had small components of protein and fat, and its most prominent component was hemicellulose at 48 wt. %. The Zein protein also had small components of ADF fiber and fat but no hemicellulose.

### 5.1.2 – Thermogravimetric Analysis

Thermogravimetric analysis (TGA) was performed on each sample that was chemically analyzed. The results presented are the percent change of weight of each sample and the first derivative of the percent change of weight. These results are presented in Figure 19.

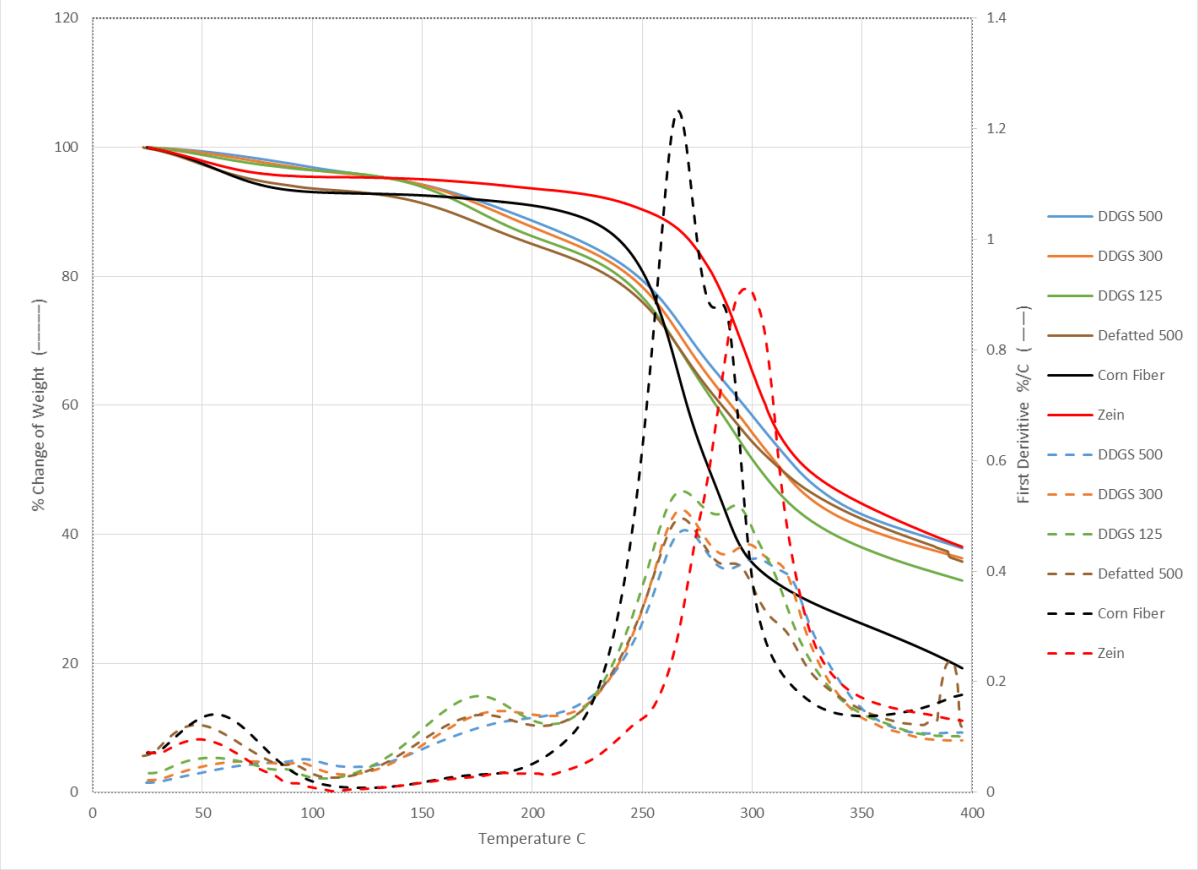


Figure 19 – Thermogravimetric Analysis Results

All the samples underwent weight loss at temperatures less than 100 ˚C. This weight loss was most likely due to moisture in the samples and, thus, considered negligible. From the first derivative curves, all samples exhibited their main degradation between 250 and 300 ˚C. This corresponds to the degradation of hemicellulose, lignin, and protein [51]. The prominent decomposition of the corn fiber occurred at 267 ˚C whereas the Zein protein

degradation peaked at 296 ˚C. The small amount of protein in the corn fiber was the most likely cause of the small degradation peak at 287 ˚C.

Among the DDGS particle sizes, there was a slight increase of the rate of degradation with the reduction of particle size. This was observed by the increased values of the first derivative. The rate of degradation increased with the decrease of the particle size. This suggests that the micronization of the DDGS had started to degrade the particles a small amount. Also, the defatted DDGS exhibited degradation similar to the normal DDGS samples.

Between 150 ˚C and 200 ˚C, the DDGS samples experienced a small peak in the first derivative of weight percent. This peak was due to the onset of the protein, hemicellulose, and lignin degradation as well as other components such as starch and fat. The onset of degradation of the protein demonstrated the decoupling of the protein had occurred. Thus, the TGA test showed that a press temperature of 200 ˚C would be suitable of achieving protein decoupling while maintaining 90 percent of the fiber by weight.

### 5.1.3 – Differential Scanning Calorimetry

Differential scanning calorimetry (DSC) was used to determine the reaction kinetics of a DDGS and MUF resin mixture. During testing, both the 5 wt. % -500 µm DDGS with 10% MUF resin and the 15 wt. % -300 µm DDGS with 10% MUF resin tests failed and, therefore, were excluded from further analysis. The initial heating of the samples is shown in Figure 20.

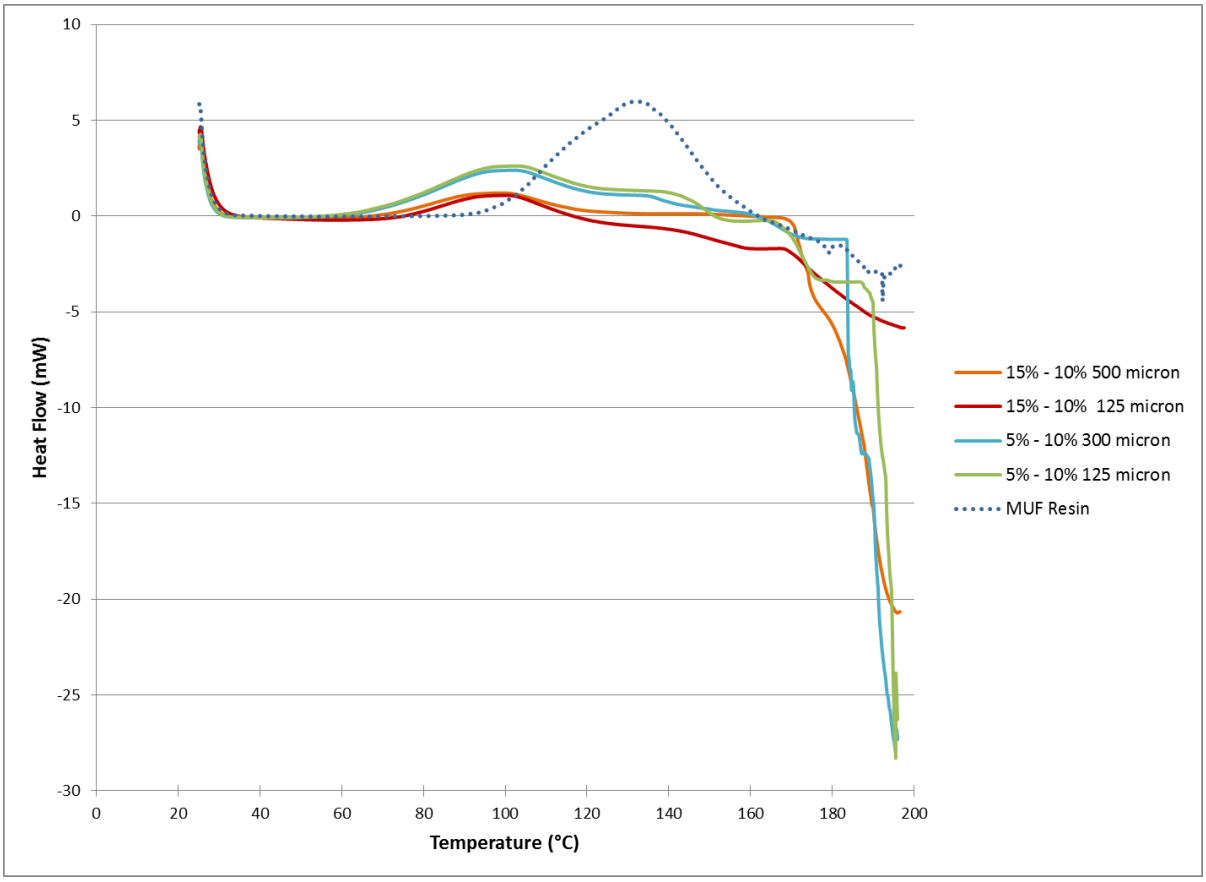


Figure 20 – DSC Curing Curves

These DSC curves depict both the exothermic and exothermic portions of the chemical reaction. The exothermic portion is shown in the positive regions on the graph and represents the MUF resin curing. The resin cured between 100 ˚C and 160 ˚C. The addition of the DDGS particles reduced the curing temperature of the resin. The endothermic portion is represented in the negative region and is caused by the fiber degradation and protein decoupling. This region was observed between 160 ˚C and 200 ˚C which corresponded to the onset of degradation observed in the TGA results.

The second heating showed the amount of cross-linking of the system. A highly cross-linked system will not experience an exothermic region.

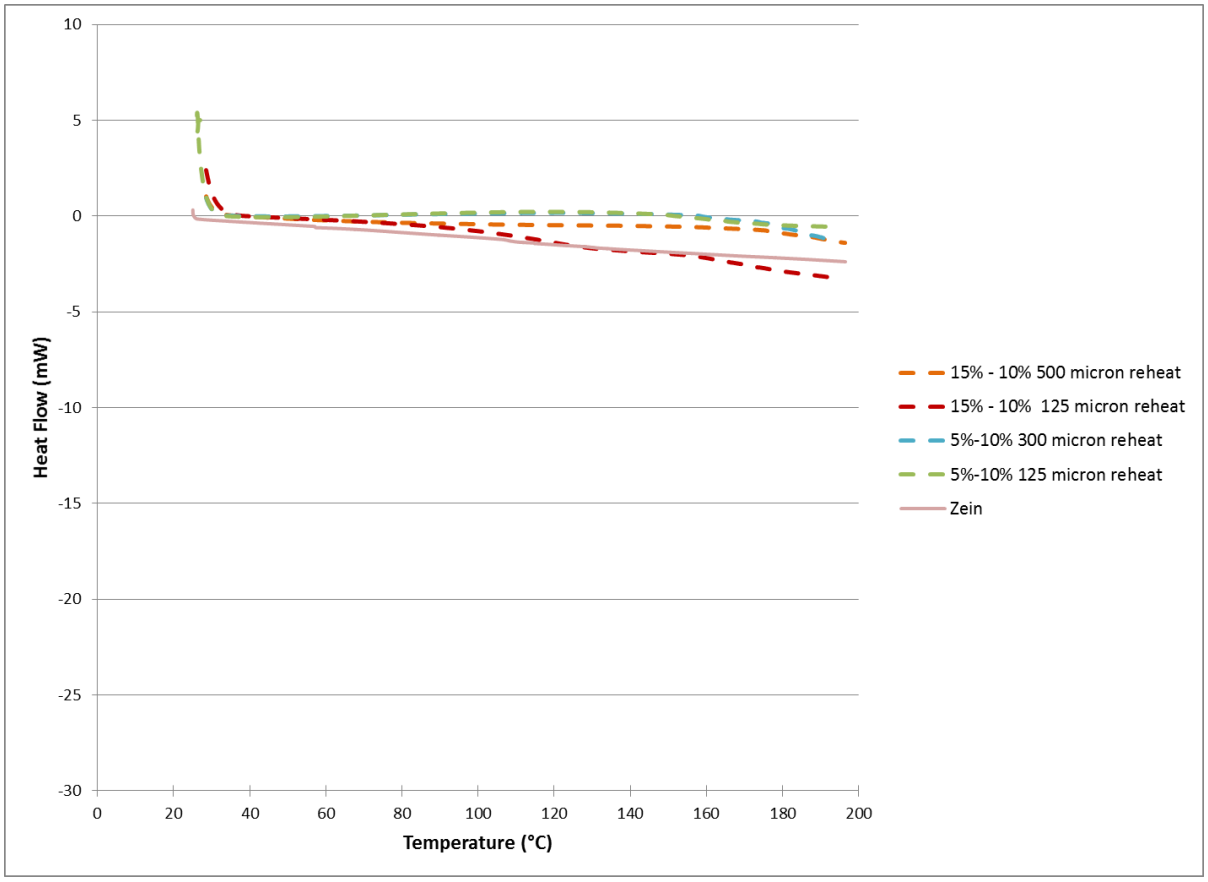


Figure 21 – DSC Second Heat

Figure 21, above, shows that the blends of DDGS and MUF resin were nearly cured. The absence of the large melt region signifies that the fiber and protein have bonded with the resin in some fashion to resist further degradation. Each curve steadily decreased indicating that the degradation did not peak at temperatures below 200 ˚C. Zein protein experienced a similar degradation corresponding to the absence of the weight loss curve and derivative from the TGA. The DSC tests demonstrated that the fiber and protein of the DDGS can decouple with heat and then further bond to the MUF resin.

### 5.1.4 – Fourier Transform Infrared Spectroscopy

FTIR was used to further determine how the MUF resin bonds with the zein protein. The structure of the MUF resin has similar functional groups of amines and amides similar

to the peptide chains of proteins. The useful peaks from the FTIR spectrum fell within 3500 $cm^{-1}$ and 1000 $cm^{-1}$ as shown in Figure 22.

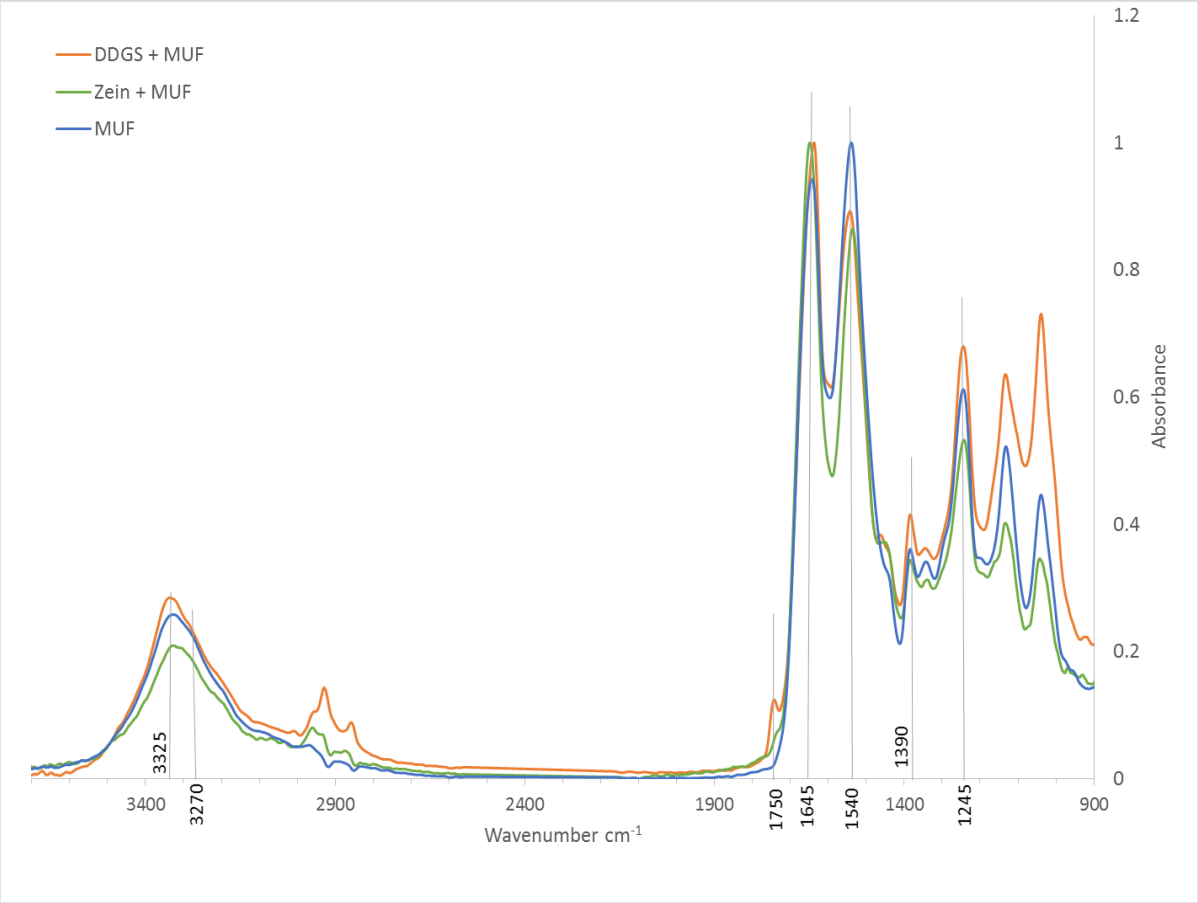


Figure 22 – FTIR Spectrum

The spectrum is very typical of nitrogen containing compounds. The first peak at 3325 $cm^{-1}$ represents hydrogen bonding between oxygen atoms and hydrogen atoms. The presence of this peak shows that hydrogen bonding occurs within the resin and also stays relatively consistent with the addition of DDGS. The elongation of the peak around 3270 $cm^{-1}$ indicates that the solutions have an N-H bond stretching. The small peaks clustered around 2900 $cm^{-1}$ are from C-H bonds from $CH_2$ groups of the carbon chain. With the addition of cellulosic materials, the increase of these peaks is expected. Other expected

peaks are the methyl group (1390 $cm^{-1}$), C-N bond of an amine (1245 $cm^{-1}$), and C-O bond of esters and alcohols (1200 – 1000 $cm^{-1}$).

The most important peaks to determine the changes of functionality fall between 1750 and 1540 $cm^{-1}$. The increase of the peak at 1750 $cm^{-1}$ shows that there is an increase of the C=O bonds from the aldehydes. The increase of the 1645 $cm^{-1}$ peak comes from the C=O bond from amides. Then the decrease at 1540 $cm^{-1}$ is characteristic of the N-H bond from amines. These results show that there is more happening than simply hydrogen bonding between amides and amines. But the actual reaction between the MUF resin and DDGS proteins cannot be determined.

## 5.2 – Mechanical and Physical Testing

This section contains the results and discussion of density, linear expansion, water absorption, flexural, internal bond, hardness, and screw withdrawal tests.

### 5.2.1 – Density Testing

The target density of the boards was 640 $kg/m^3$ which is the upper limit of low-density particleboards. The density of each board produced was calculated according to ASTM D2395.

Figure 23 shows that there was a slight spread in the density, but the bulk of the boards were still considered low-density particleboards. Two boards of the 15 wt. % and 300 and 500 micron particle sizes and the control board were greater than the 640 $kg/m^3$ target density.

Samples for further testing were taken at random from the four panels. This contributed slightly to the spread of the data. During the analysis of the tests, the density of each panel and the average density of the batch were considered as variables. Neither the density of individual panels nor the average density proved to be a significant variable

in the analysis. This suggested that the spread of the densities was not a significant factor affecting the mechanical properties and thus could be eliminated in further analyses.

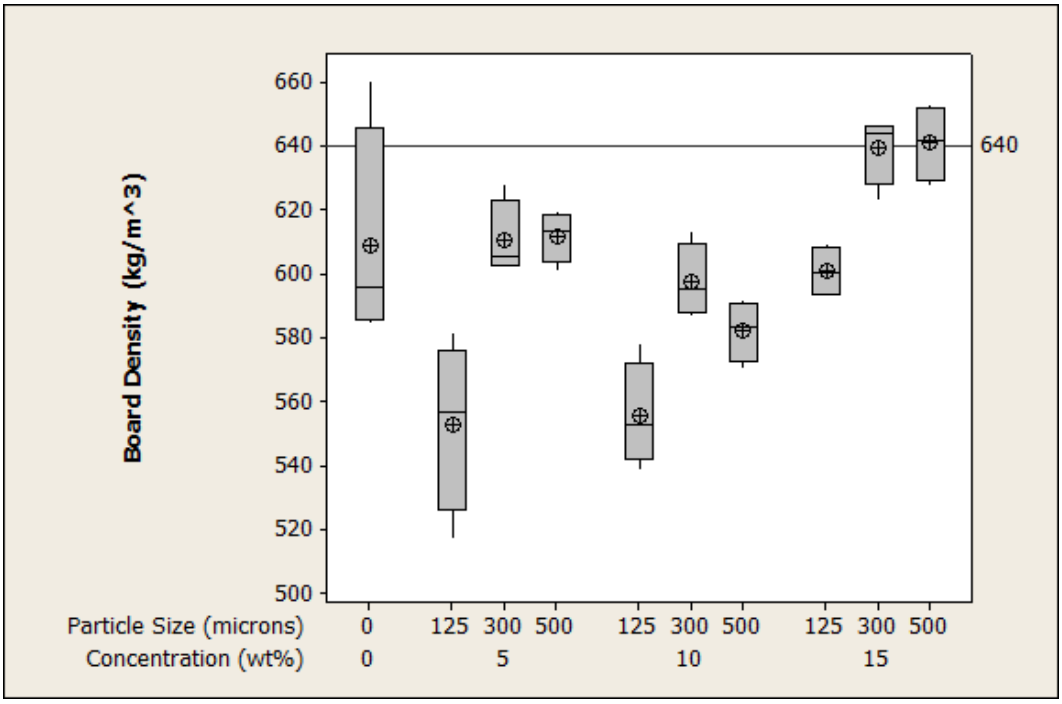


Figure 23 – Boxplot of Panel Density

### 5.2.2 – Linear Expansion

To test the linear expansion of the boards, five samples were tested. The desired outcome is the most dimensionally stable sample which means the smallest linear expansion. The sample expansion varied from 0 to 4 mm, and the percent change of length is provided in Figure 24. The results showed good dimensional stability in the 5 wt. % and 10 wt. % blends but an increase in the linear dimension with the 15 wt. % loading.

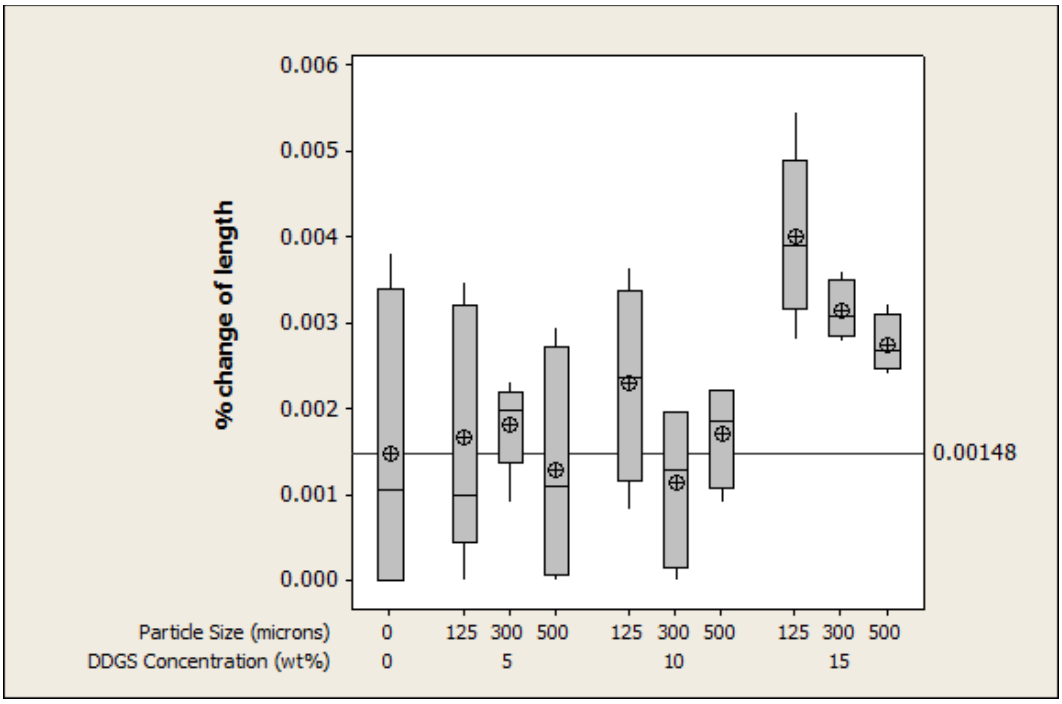


Figure 24 – Boxplot of Linear Expansion Results

The two-way t test (Table 9) showed that only the 15 wt. % - 125 µm was statistically different from the control sample. This sample had an increased expansion which is undesirable.

Table 9 – Two-Way T Test of Linear Expansion Tests

| Sample Concentration | Sample Particle Size | t - value | P - value |
|---|---|---|---|
| 0 | 0 | 0 | 1 |
| 5 | 125 | -0.15 | 0.885 |
| 5 | 300 | -0.35 | 0.749 |
| 5 | 500 | 0.16 | 0.877 |
| 10 | 125 | -0.74 | 0.49 |
| 10 | 300 | 0.33 | 0.758 |
| 10 | 500 | -0.23 | 0.83 |
| 15 | 125 | -2.46 | 0.07 |
| 15 | 300 | -1.76 | 0.176 |
| 15 | 500 | -1.34 | 0.272 |

The ANOVA of the linear expansion (Table 10) showed that only the concentration-concentration interaction effect was significant.

Table 10 – ANOVA of Linear Expansion Tests

| | DF | Seq SS | Adj SS | Adj MS | F | P |
|---|---|---|---|---|---|---|
| Regression | 5 | 0.00003 | 0.00003 | 0.000006 | 6.38 | 0 |
| Linear | 2 | 0.000024 | 0.000002 | 0.000001 | 0.88 | 0.425 |
| DDGS Concentration | 1 | 0.00002 | 0.000001 | 0.000001 | 1.53 | 0.225 |
| Particle Size | 1 | 0.000004 | 0 | 0 | 0.35 | 0.558 |
| Square | 2 | 0.000005 | 0.000005 | 0.000003 | 2.69 | 0.083 |
| Concentration^2 | 1 | 0.000005 | 0.000005 | 0.000005 | 4.84 | 0.035 |
| Particle size^2 | 1 | 0 | 0 | 0 | 0.54 | 0.469 |
| Interaction | 1 | 0.000001 | 0.000001 | 0.000001 | 0.99 | 0.327 |
| Concentration*Particle Size | 1 | 0.000001 | 0.000001 | 0.000001 | 0.99 | 0.327 |
| Residual error | 33 | 0.000031 | 0.000031 | 0.000001 | | |
| Lack of Fit | 3 | 0.000002 | 0.000002 | 0.000001 | 0.79 | 0.511 |
| Pure Error | 30 | 0.000028 | 0.000028 | 0.000001 | | |
| Total | 38 | 0.00006 | | | | |

The model, with an R Squared of 0.491, showed that the variables have very little effect on the expansion (Table 11).

Table 11 – Model of Linear Expansion Results

| Term | Coefficient | P Value |
|---|---|---|
| Constant | 3.3 E-3 | 0.041 |
| Concentration | -0.3 E-3 | 0.225 |
| Particle Size | -4 E-6 | 0.558 |
| **Concentration^2** | **2.9 E-5** | **0.035** |
| Particle Size^2 | 0 | 0.469 |
| Concentration*Particle Size | 0 | 0.327 |
| R-Squared = 0.491 | | |

Figure 25 shows contour plot created from this model. It identified that the 5 wt. % - 300 µm DDGS filler produced the most dimensionally stable particleboard. Its properties were comparable to the control sample as seen in Figure 24. However, all of the batches were statistically equivalent to the control sample except the 15 wt. % blends. Thus, the addition of DDGS did not benefit nor deter from the linear expansion of particleboards.

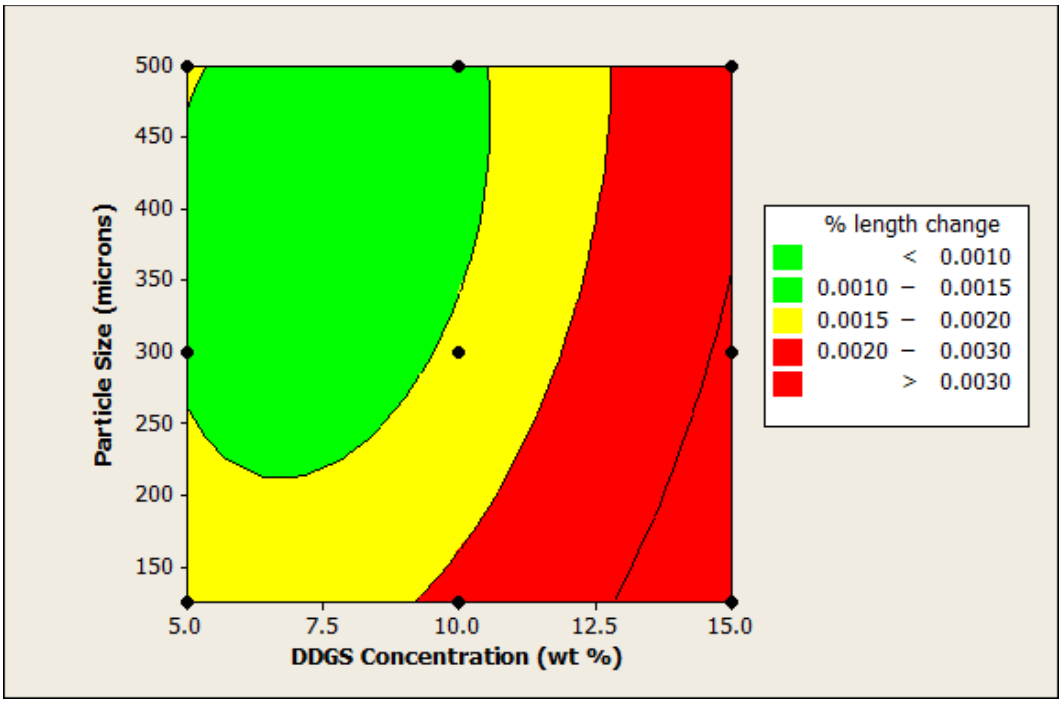


Figure 25 – Contour Plot of Linear Expansion Model

### 5.2.3 – Water Absorption

During the water absorption tests, five samples from each blend were tested. Lignocellulosic materials absorb water fastest in the first several hours. Because of this, the samples were measured for mass and volume change at 2 and 24 hours. The change of mass and the volume are discussed in separate sections.

#### 5.2.3.1 – Mass Change

The 0- to 2-hour mass change is shown in Figure 26. The results showed that the mass due to water absorption was roughly comparable to the control sample in the case of 5 wt. % and 10 wt. %. The 15 wt. % concentrations increased more than the control sample as did the 5 wt. % - 300 µm sample.

After 24 hours, the samples became saturated as depicted in Figure 27. In all cases, the mass change increased, compared to the control sample, except the 5 wt. % - 500 µm blend. This blend still had a lower mean value than the control sample.

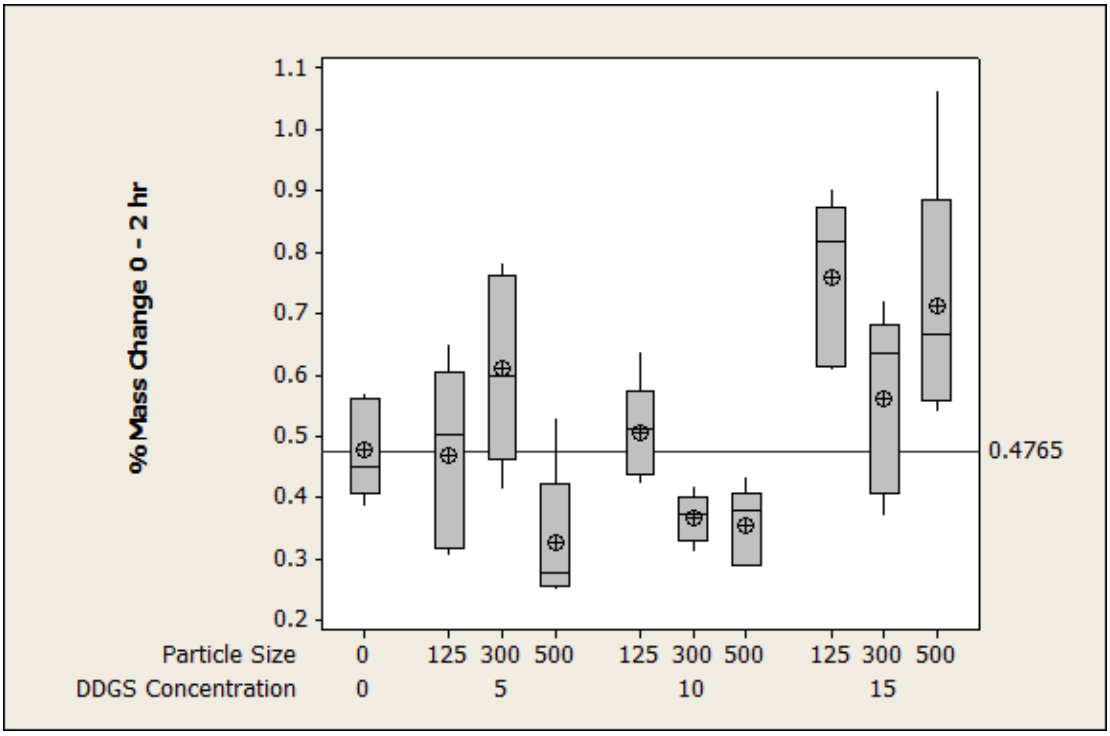


Figure 26 – Boxplot of 2-Hour Mass Change

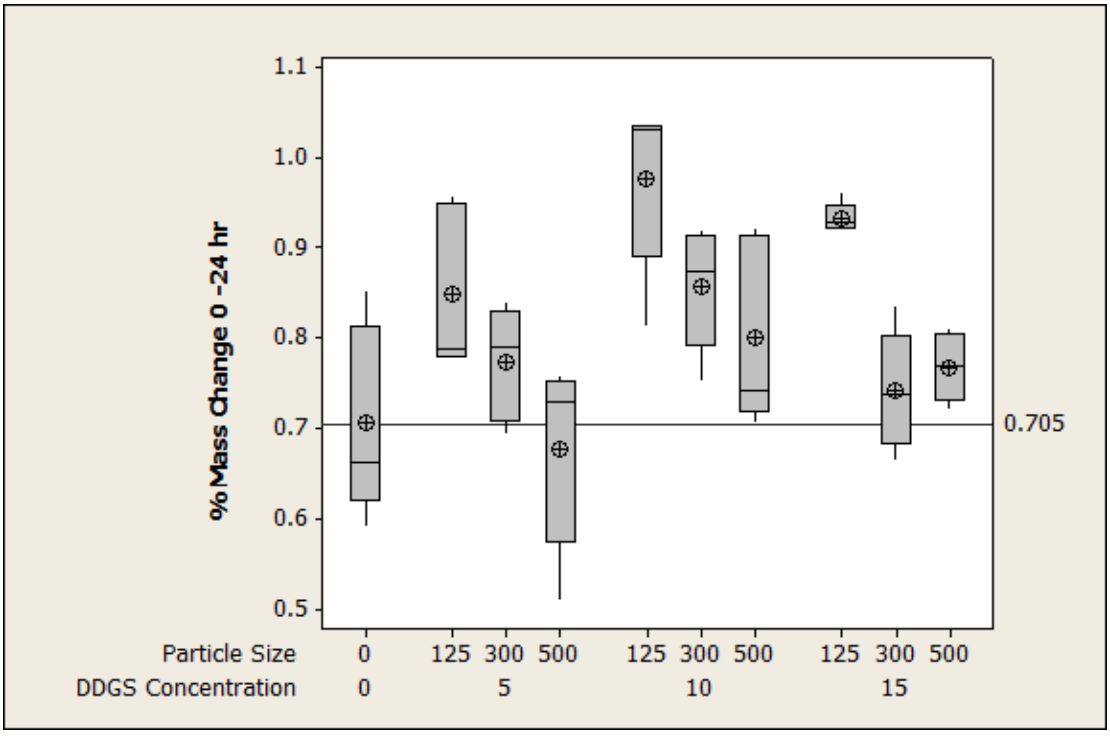


Figure 27 – Boxplot of 24-Hour Mass Change

The two-way t tests for the 2- and 24-hour mass change experiments are provided in Table 12 and Table 13, respectively.

Table 12 – Two-Way T Test for 2-Hour Mass Change

| Sample Concentration | Sample Particle Size | t - value | P - value |
|---|---|---|---|
| 0 | 0 | 0 | 1 |
| 5 | 125 | 0.11 | 0.916 |
| 5 | 300 | -1.69 | 0.142 |
| 5 | 500 | 2.38 | 0.049 |
| 10 | 125 | -0.57 | 0.589 |
| 10 | 300 | 2.74 | 0.041 |
| 10 | 500 | 2.67 | 0.032 |
| 15 | 125 | -3.98 | 0.007 |
| 15 | 300 | -1.13 | 0.301 |
| 15 | 500 | -2.34 | 0.067 |

Table 13 – Two-Way T Test for 24-Hour Mass Change

| Sample Concentration | Sample Particle Size | t - value | P - value |
|---|---|---|---|
| 0 | 0 | 0 | 1 |
| 5 | 125 | -2.3 | 0.055 |
| 5 | 300 | -1.24 | 0.262 |
| 5 | 500 | 0.44 | 0.674 |
| 10 | 125 | -4.26 | 0.004 |
| 10 | 300 | -2.71 | 0.035 |
| 10 | 500 | -1.45 | 0.191 |
| 15 | 125 | -4.78 | 0.009 |
| 15 | 300 | -0.65 | 0.54 |
| 15 | 500 | -1.25 | 0.268 |

In both the 2-hour and 24-hour mass changes, only the 10 wt. % and 15 wt. % at 125 µm were significantly different from the control sample. The rest of the samples were statistically equivalent.

The models created from the ANOVA analysis showed that the 2-hour mass increase did not result in any significant variables (Table 14). The 24-hour test showed that the concentration, particle size main effect, and concentration squared effects were significant (Table 15).

Table 14 – Model of 2-Hour Mass Change

| Term | Coefficient | P Value |
|---|---|---|
| Constant | 0.1811 | 0.004 |
| Concentration | 0.0159 | 0.129 |
| Particle Size | 0.0001 | 0.547 |
| Concentration^2 | -0.0005 | 0.300 |
| Particle Size^2 | 0 | 0.292 |
| Concentration*Particle Size | 0 | 0.294 |
| R-Squared = 0.447 | | |

Table 15 – Model of 24-Hour Mass Change

| Term | Coefficient | P Value |
|---|---|---|
| Constant | 0.7323 | 0 |
| **Concentration** | **0.0743** | **0.001** |
| **Particle Size** | **-0.0014** | **0.008** |
| **Concentration^2** | **-0.0035** | **0.001** |
| Particle Size^2 | 0 | 0.055 |
| Concentration*Particle Size | 0 | 0.861 |
| R-Squared = 0.582 | | |

#### 5.2.3.2 – Volume Change

The volume change results from 0 to 2 hours (Figure 28) showed that the volume changes of the 5 wt. % and 10 wt. % samples were reduced from the control sample. The 15 wt. % DDGS samples also exhibited a reduced volume change from the control sample but were closer to the control mean.

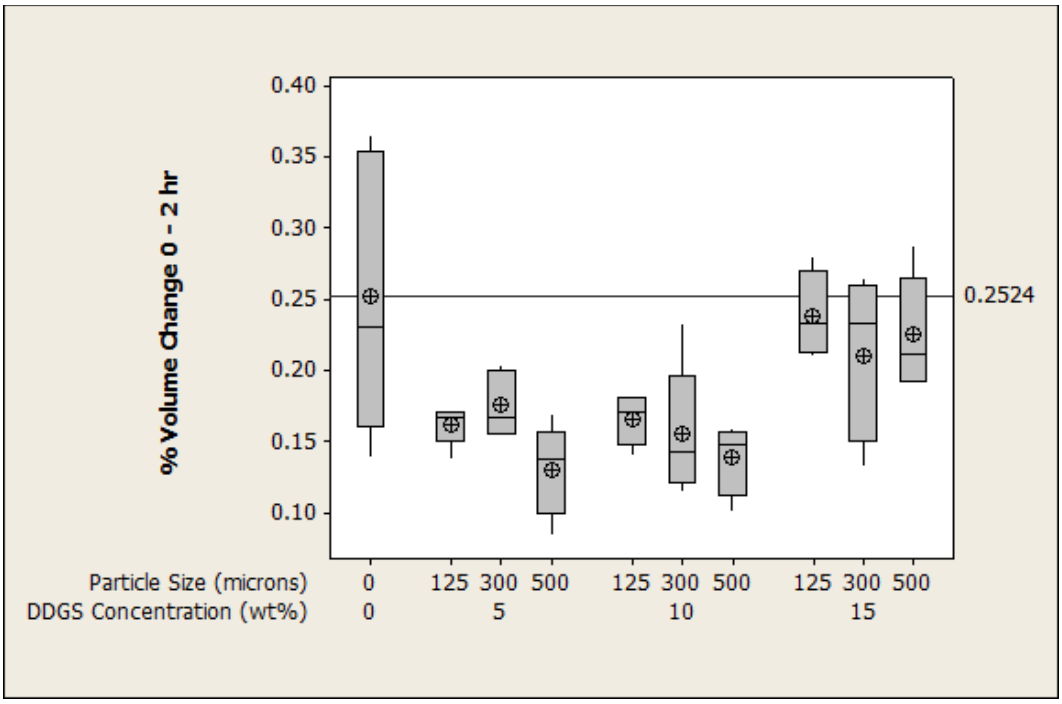


Figure 28 – Boxplot of 2-Hour Volume Change

The 24-hour volume change (Figure 29) represents the saturated state of the boards.

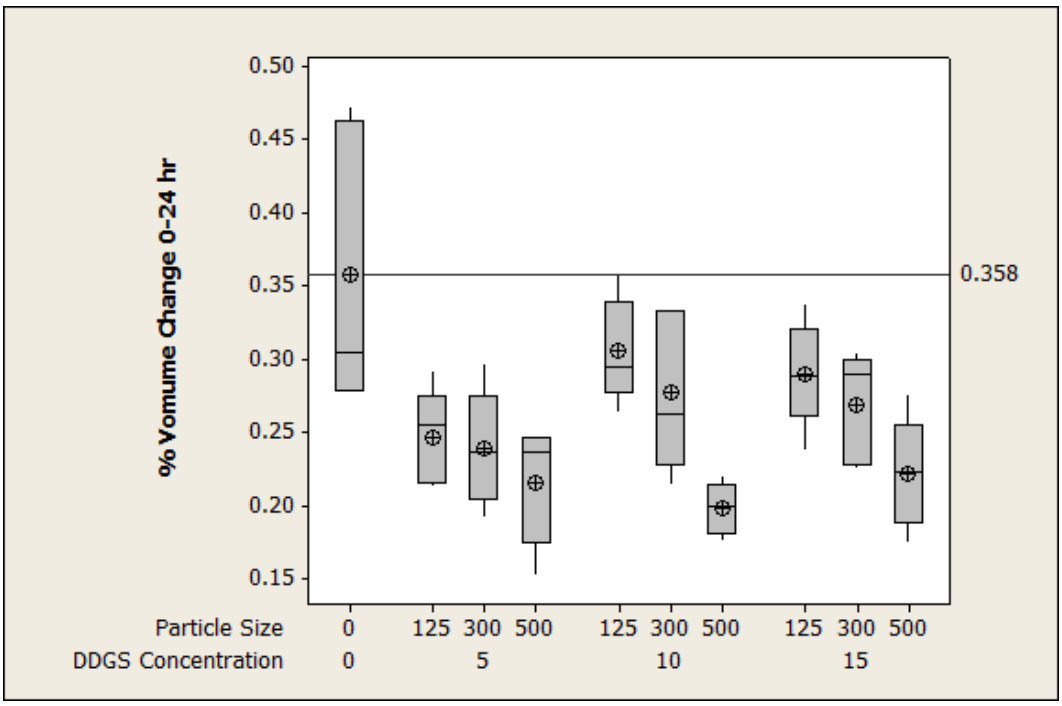


Figure 29 – Boxplot of 24-Hour Volume Change

Figure 29 shows that as time increased, all samples exhibited less volume change than the control sample. This indicates that the addition of the DDGS did not affect the volume change of the sample.

The t test of the 2-hour volume change showed that all the samples were statistically equivalent to the control sample (Table 16). With the full 24 hours of testing, the t test showed that all the batches with 500 µm were statistically different from the control sample (Table 17). These samples exhibited less volume change and demonstrated that the addition of the larger particle size of DDGS positively affected the volume change of the particleboards.

ANOVA was conducted for the 2-hour and 24-hour tests, and a model was created for each (Table 18 and Table 19, respectively). The model showed that in both cases the concentration and concentration squared interaction were significant.

Table 16 – Two-Way T Test of 2-Hour Volume Change

| Sample Concentration | Sample Particle Size | t - value | P - value |
|---|---|---|---|
| 0 | 0 | 0 | 1 |
| 5 | 125 | 2.02 | 0.114 |
| 5 | 300 | 1.68 | 0.168 |
| 5 | 500 | 2.61 | 0.059 |
| 10 | 125 | 1.92 | 0.128 |
| 10 | 300 | 1.97 | 0.106 |
| 10 | 500 | 2.44 | 0.071 |
| 15 | 125 | 0.28 | 0.792 |
| 15 | 300 | 0.81 | 0.449 |
| 15 | 500 | 0.56 | 0.599 |

Table 17 – Two-Way T Test of 24-Hour Volume Change

| Sample Concentration | Sample Particle Size | t - value | P - value |
|---|---|---|---|
| 0 | 0 | 0 | 1 |
| 5 | 125 | 2.42 | 0.073 |
| 5 | 300 | 2.53 | 0.052 |
| 5 | 500 | 3.02 | 0.029 |
| 10 | 125 | 1.14 | 0.307 |
| 10 | 300 | 1.63 | 0.155 |
| 10 | 500 | 3.62 | 0.022 |
| 15 | 125 | 1.45 | 0.205 |
| 15 | 300 | 1.9 | 0.116 |
| 15 | 500 | 2.91 | 0.033 |

Table 18 – Model of 2-Hour Volume Change

| Term | Coefficient | P Value |
|---|---|---|
| Constant | 0.2615 | 0 |
| **Concentration** | **-0.0241** | **0.016** |
| Particle Size | -0.0001 | 0.778 |
| **Concentration^2** | **0.0015** | **0.003** |
| Particle Size^2 | 0 | 0.777 |
| Concentration*Particle Size | 0 | 0.502 |
| R-Squared = 0.517 | | |

Table 19 – Model of 24-Hour Volume Change

| Term | Coefficient | P Value |
|---|---|---|
| Constant | 1.065 | 0 |
| **Concentration** | **-0.119** | **0.005** |
| Particle Size | -0.0008 | 0.390 |
| **Concentration^2** | **0.0065** | **0.001** |
| Particle Size^2 | 0 | 0.802 |
| Concentration*Particle Size | 0 | 0.408 |
| R-Squared = 0.445 | | |

### 5.2.3.3 – Water Absorption Contour Plots

The contour plots from the four analyses were plotted and, in the case of the 2-hour test and 24-hour test, the mass contour and volume contour plot were overlaid on each other. In each case, minimizing the percent change was preferred.

In the case of the 2-hour test, the shaded region of Figure 30 shows the regions that are outside the ideal conditions. Within the white region are the predicted optimum blends. Results showed that panels up to 10 wt. % - 500 microns were predicted to perform the best.

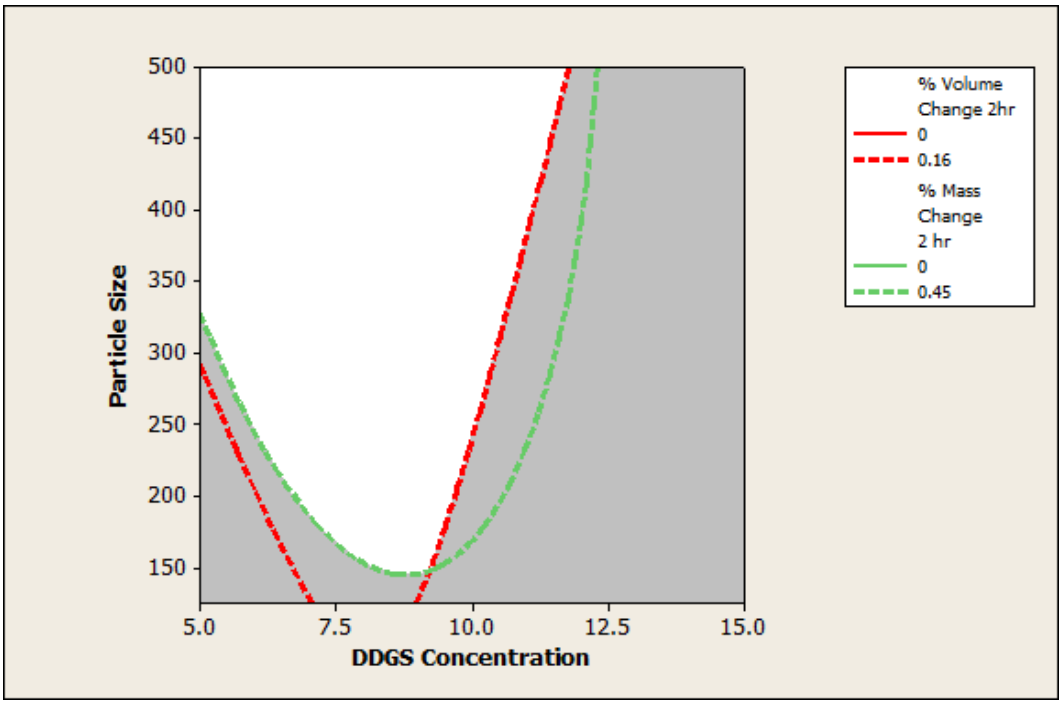


Figure 30 – Overlaid Contour Plot of Water Absorption 2-Hour Test

The 24-hour overlaid contour plot identified a saddle. The ideal regions were split as indicated by the white regions of Figure 31. The ideal regions were centered around 5 wt. % and 15 wt. % at 500 µm.

Independent of the time of exposure, both cases showed that panels with 5 wt. % DDGS filler and 500 µm particle size would produce the best results by minimizing volume change and mass change. The trend toward the higher particle size may be due to the

processing. With the micronization of the DDGS particles, the surface area increased which would allow for more water absorption with smaller particle sizes.

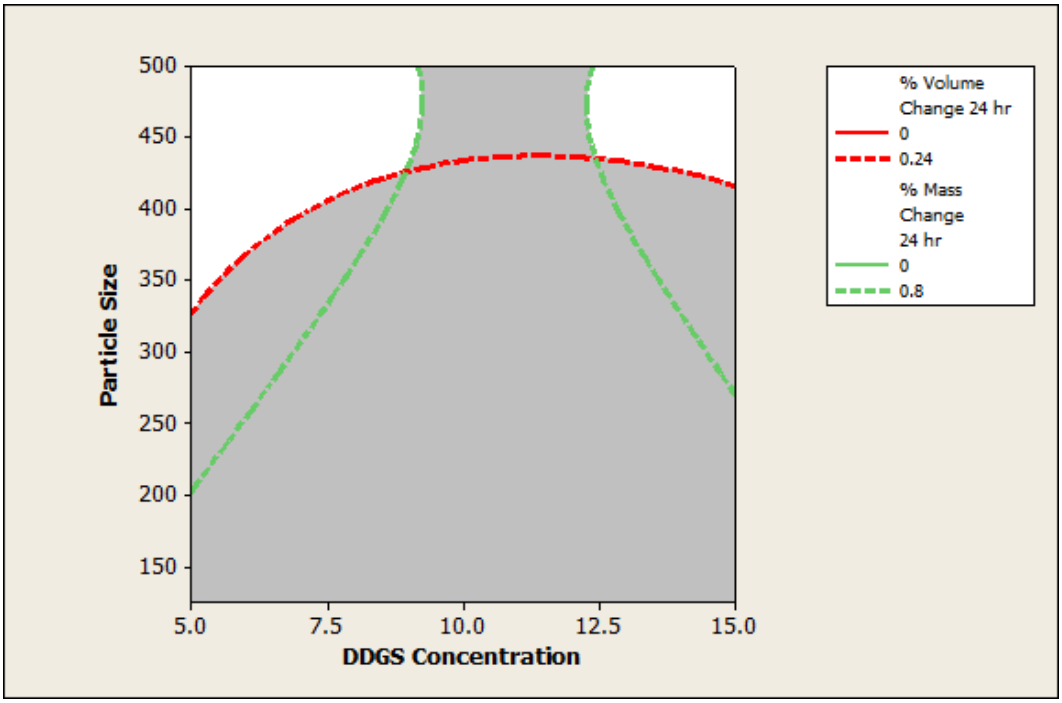


Figure 31 – Overlaid Contour Plot for 24-Hour Water Absorption

### 5.2.4 – Static Bend Testing

Flexural testing was performed to determine the effect of the DDGS concentration and particle size on the modulus of elasticity and modulus of rupture. For both the modulus of elasticity and the modulus of rupture, an increase in the modulus compared to the control board is desired.

Five samples from each blend were tested, and the modulus of elasticity and modulus of rupture were determined. ANOVA was used to determine the significant variables, and a contour plot was created from the analysis.

### 5.2.4.1 – Modulus of Elasticity

The modulus of elasticity represents the stiffness of the beam. In the boxplot of the elastic modulus (Figure 32), the mean modulus of the control sample is represented by the horizontal line at 226.8 MPa.

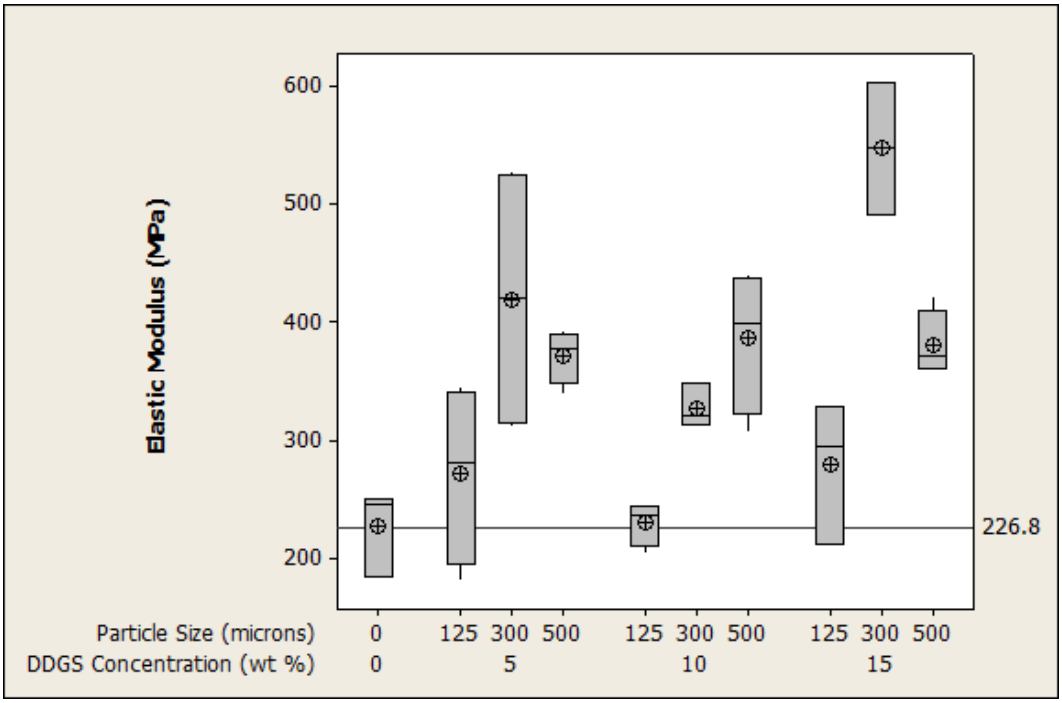


Figure 32 – Boxplot of Modulus of Elasticity

The boxplot results showed a general increase of the elastic modulus with the addition of DDGS (Figure 25). The t test compared experimental samples to the control samples, and showed that the 300 µm and 500 µm filled samples were statistically different from the control sample (Table 20).

The ANOVA analysis showed that the particle size main effect, concentration-concentration interaction effect, and particle size-particle size interaction effect were significant at the 95% confidence level (Table 21).

Table 20 – Two-Way T Test of Modulus of Elasticity

| Sample Concentration | Sample Particle Size | T- value | P - value |
|---|---|---|---|
| 0 | 0 | 0 | 1 |
| 5 | 125 | -1.03 | 0.363 |
| 5 | 300 | -3.09 | 0.054 |
| 5 | 500 | -5.97 | 0.009 |
| 10 | 125 | -0.16 | 0.889 |
| 10 | 300 | -4.21 | 0.052 |
| 10 | 500 | -4.24 | 0.013 |
| 15 | 125 | -1.28 | 0.291 |
| 15 | 300 | -8.31 | 0.004 |
| 15 | 500 | -6.01 | 0.009 |

Table 21 – ANOVA of Modulus of Elasticity

| | DF | Seq SS | Adj SS | Adj MS | F | P |
|---|---|---|---|---|---|---|
| Regression | 5 | 196974 | 196974 | 39395 | 7.78 | 0 |
| Linear | 2 | 80666 | 132041 | 66021 | 13.03 | 0 |
| DDGS Concentration | 1 | 9527 | 16947 | 16947 | 3.34 | 0.078 |
| Particle Size | 1 | 71138 | 101764 | 101764 | 20.08 | 0 |
| Square | 2 | 116247 | 116201 | 58101 | 11.47 | 0 |
| Concentration^2 | 1 | 27420 | 23007 | 23007 | 4.54 | 0.042 |
| Particle size^2 | 1 | 88827 | 88614 | 88614 | 17.49 | 0 |
| Interaction | 1 | 61 | 61 | 61 | 0.01 | 0.913 |
| Concentration*Particle Size | 1 | 61 | 61 | 61 | 0.01 | 0.913 |
| Residual error | 27 | 136800 | 136800 | 5067 | | |
| Lack of Fit | 3 | 46896 | 46896 | 15632 | 4.17 | 0.016 |
| Pure Error | 24 | 89904 | 89904 | 3746 | | |
| Total | 32 | 333775 | | | | |

The model created from the ANOVA test showed that the most influential components were the particle size and squared iteration of the concentration (Table 22).

Table 22 – Model of Modulus of Elasticity

| Term | Coefficient | P Value |
|---|---|---|
| Constant | 158.8 | 0.222 |
| Concentration | -39.9 | 0.078 |
| **Particle Size** | **2.354** | **0** |
| **Concentration^2** | **2.249** | **0.042** |
| **Particle Size^2** | **-0.003** | **0** |
| Concentration*Particle Size | -0.002 | 0.913 |
| R-Squared = 0.59 | | |

A contour plot (Figure 33) was created to determine the interactions between the particle size and concentration.

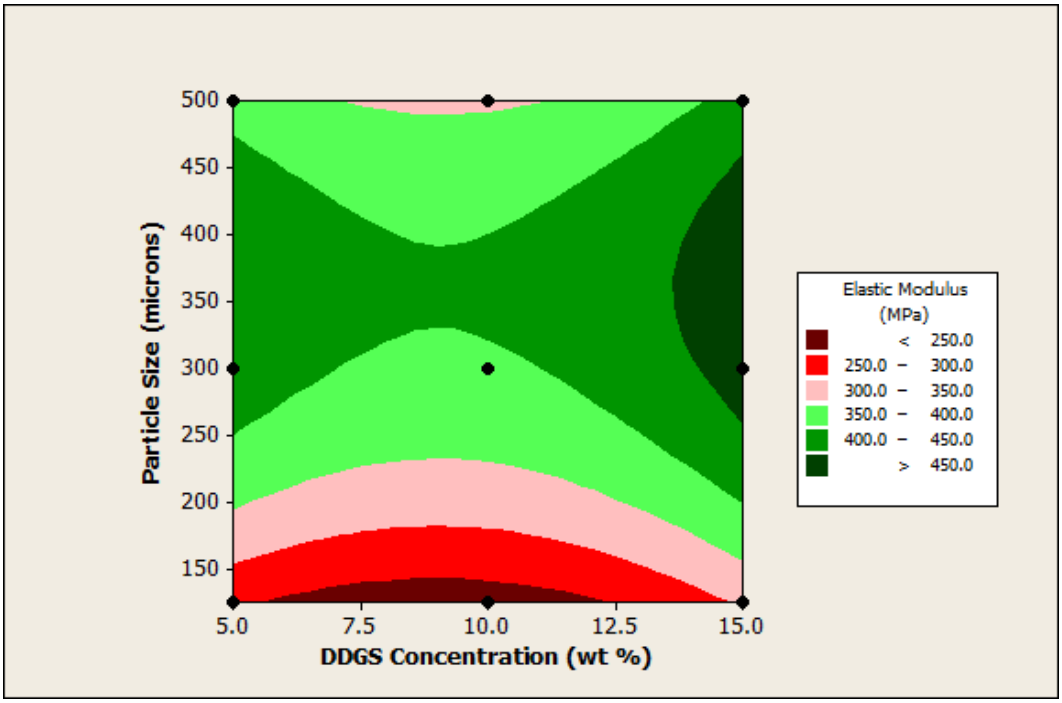


Figure 33 – Contour Plot of Modulus of Elasticity

In this model, each dot signifies a design point representing a tested blend. The mean control elastic modulus value was used as the low end bound, thus represented by the crimson portion of the graph.

The model showed that the superior concentration and particle size interaction was 15 wt. % - 300 microns followed closely by 5 wt. % - 300 microns. The smaller particles did not improve the elastic modulus which would have been expected since it has been shown that smaller particle sizes improve the load transfer and thus stiffens the material.

#### 5.2.4.2 – Modulus of Rupture

The modulus of rupture is the maximum stress that a material can experience while resisting deformation. In Figure 34, the modulus of rupture results are displayed, and the mean of the control sample is represented by the horizontal line.

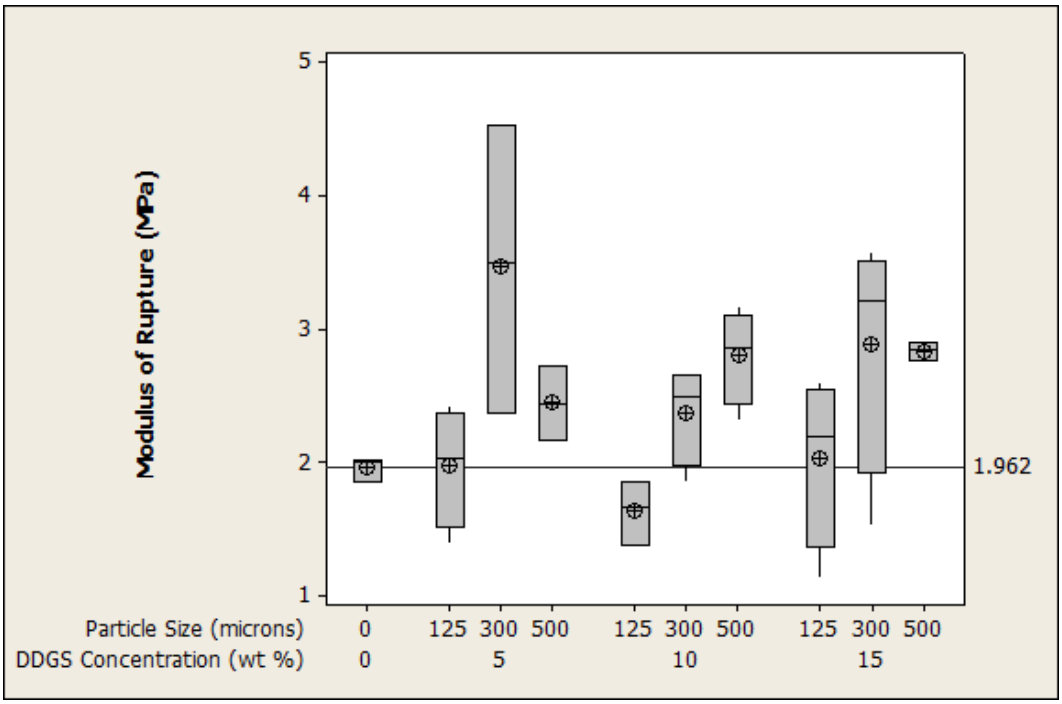


Figure 34 – Boxplot of Modulus of Rupture

Similar to the modulus of elasticity, the modulus of rupture increased with the addition of DDGS filler. The standard deviation of the data also increased with the addition of DDGS filler. This indicates that the addition of the DDGS filler in the boards decreases the homogeny of the boards.

The t test of the means showed that the 10 wt. % and 15 wt. % samples at 500 µm were statistically different from the mean (Table 23). While the 5 wt. % - 300 µm blend had the largest difference between means, its large standard deviation caused the sample to be statistically equivalent to the control sample.

Table 23 – Two-Way T Test of Modulus of Rupture

| Sample Concentration | Sample Particle Size | T- value | P - value |
|---|---|---|---|
| 0 | 0 | 0 | 1 |
| 5 | 125 | -0.04 | 0.967 |
| 5 | 300 | -2.41 | 0.138 |
| 5 | 500 | -2.87 | 0.064 |
| 10 | 125 | 2.23 | 0.155 |
| 10 | 300 | -2.12 | 0.124 |
| 10 | 500 | -4.48 | 0.021 |
| 15 | 125 | -0.21 | 0.844 |
| 15 | 300 | -1.98 | 0.141 |
| 15 | 500 | -13.41 | 0.001 |

The ANOVA test identified the linear particle size interaction and the squared particle size interaction as significant variables in the model (Table 24).

Table 24 – ANOVA of Modulus of Rupture

| | DF | Seq SS | Adj SS | Adj MS | F | P |
|---|---|---|---|---|---|---|
| Regression | 5 | 6.6176 | 6.6176 | 1.3235 | 3.79 | 0.01 |
| Linear | 2 | 3.2489 | 3.637 | 1.8185 | 5.2 | 0.012 |
| DDGS Concentration | 1 | 0.0081 | 0.8153 | 0.8153 | 2.33 | 0.138 |
| Particle Size | 1 | 3.2407 | 2.7354 | 2.7354 | 7.83 | 0.009 |
| Square | 2 | 3.2375 | 3.2417 | 1.6209 | 4.64 | 0.018 |
| Concentration^2 | 1 | 0.5528 | 0.718 | 0.718 | 2.05 | 0.163 |
| Particle size^2 | 1 | 2.6846 | 2.6881 | 2.6881 | 7.69 | 0.01 |
| Interaction | 1 | 0.1313 | 0.1313 | 0.1313 | 0.38 | 0.545 |
| Concentration*Particle Size | 1 | 0.1313 | 0.1313 | 0.1313 | 0.38 | 0.545 |
| Residual error | 28 | 9.7868 | 9.7868 | 0.3495 | | |
| Lack of Fit | 3 | 1.8664 | 1.8664 | 0.6221 | 1.96 | 0.145 |
| Pure Error | 25 | 7.9204 | 7.9204 | 0.3168 | | |
| Total | 33 | 16.4044 | | | | |

The model showed that the particle-size main effect and the particle size – particle size interaction were significant at a 95% confidence level and an R – squared value of 0.403 (Table 25).

Table 25 – Model of Modulus of Rupture

| Term | Coefficient | P Value |
|---|---|---|
| Constant | 1.87 | 0.076 |
| Concentration | -0.280 | 0.138 |
| **Particle Size** | **0.012** | **0.009** |
| Concentration^2 | 0.012 | 0.163 |
| **Particle Size^2** | **-2 E-5** | **0.010** |
| Concentration*Particle Size | 1 E-4 | 0.545 |
| R-Squared = 0.403 | | |

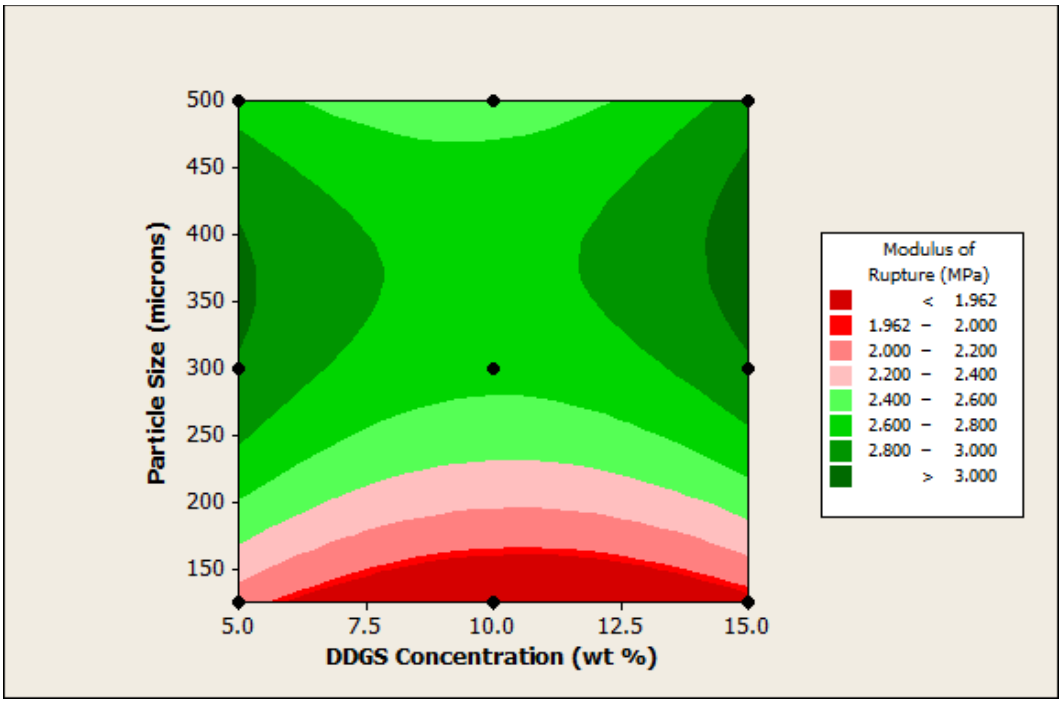


Figure 35 – Contour Plot of Modulus of Rupture

The contour plot from the model (Figure 35) showed that the superior blends are the 15 wt. % or the 5 wt. % at 300 and 500 µm. With the knowledge from the Student's t test, the blend that would produce a statistically larger mean modulus of rupture would be a DDGS filler of 15 wt. % - 500 µm.

### 5.2.5 – Internal Bond Testing

The internal bond test determines the cohesive strength of a board. An increase of the internal bond strength compared to the control board is desired. Twelve samples from each blend were tested. Twelve samples were randomly cut from the flexural test sample, and six samples were cut randomly from the linear expansion samples. The results from the internal bond tests are provided in Figure 36.

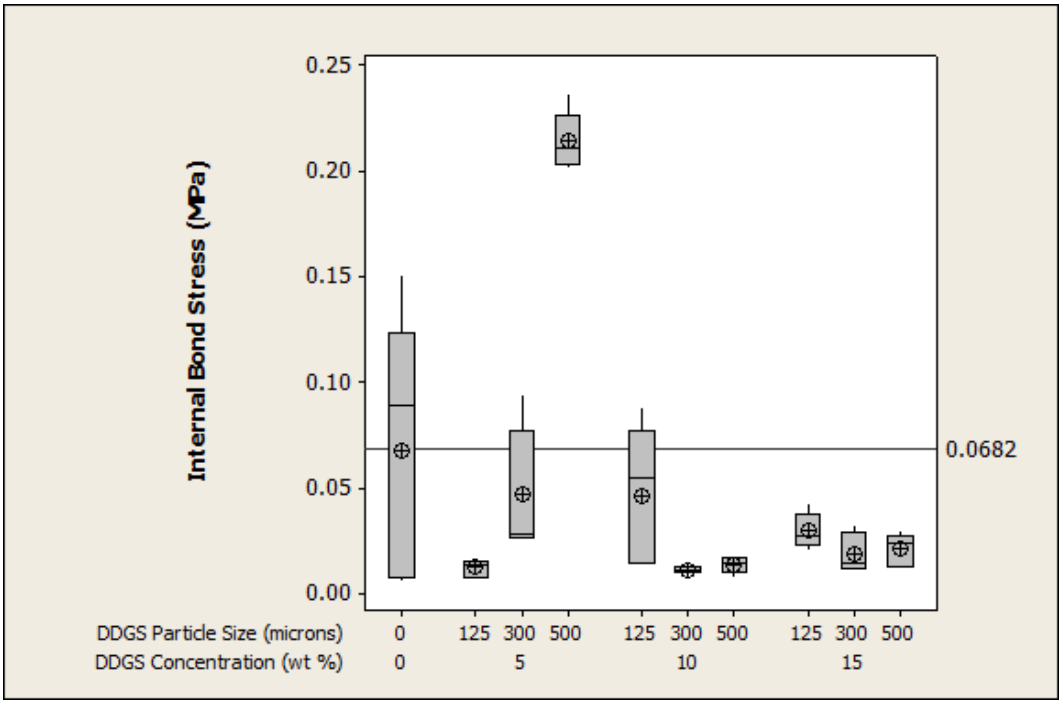


Figure 36 – Boxplot of Internal Bond Testing

The addition of DDGS filler decreased the mean internal bond strength of each sample. The addition of DDGS also decreased the standard deviation of the sample compared to the control sample.

The Student's t test results are shown in Table 26. In this analysis, the mean of each batch was compared to the mean of the control sample. P values less than 0.05 indicated that sample panels were statistically different from the control sample. This test showed that the 5 wt. % - 500 µm had a statistically higher mean value than the control sample whereas the other statistically different blends demonstrated a lower mean internal bond strength than the control sample.

Table 26 – Two-Way T Test of Internal Bond Results

| Sample Concentration | Sample Particle Size | t - value | P - value |
|---|---|---|---|
| 0 | 0 | 0 | 1 |
| 5 | 125 | 2.75 | 0.025 |
| 5 | 300 | 0.88 | 0.399 |
| 5 | 500 | -6.94 | 0 |
| 10 | 125 | 0.92 | 0.337 |
| 10 | 300 | 2.81 | 0.023 |
| 10 | 500 | 2.68 | 0.028 |
| 15 | 125 | 1.88 | 0.097 |
| 15 | 300 | 2.43 | 0.041 |
| 15 | 500 | 2.29 | 0.052 |

The ANOVA tests (Table 27) identified the significant variables. These tests showed that the squared and interaction effects between the DDGS concentration and particle size were significant.

Table 27 – ANOVA of Internal Bond Data

| | DF | Seq SS | Adj SS | Adj MS | F | P |
|---|---|---|---|---|---|---|
| Regression | 5 | 0.130427 | 0.130427 | 0.026085 | 23.88 | 0 |
| Linear | 2 | 0.052818 | 0.005443 | 0.002722 | 2.49 | 0.094 |
| DDGS Concentration | 1 | 0.033031 | 0.003676 | 0.003676 | 3.37 | 0.073 |
| Particle Size | 1 | 0.019788 | 0.001077 | 0.001077 | 0.99 | 0.326 |
| Square | 2 | 0.017083 | 0.019102 | 0.009551 | 8.74 | 0.001 |
| Concentration^2 | 1 | 0.009422 | 0.011634 | 0.011634 | 10.65 | 0.002 |
| Particle size^2 | 1 | 0.007661 | 0.008679 | 0.008679 | 7.94 | 0.007 |
| Interaction | 1 | 0.060526 | 0.060526 | 0.060526 | 55.41 | 0 |
| Concentration*Particle Size | 1 | 0.060526 | 0.060526 | 0.060526 | 55.41 | 0 |
| Residual error | 47 | 0.051344 | 0.051344 | 0.001092 | | |
| Lack of Fit | 3 | 0.039692 | 0.039692 | 0.013231 | 49.96 | 0 |
| Pure Error | 44 | 0.011652 | 0.011652 | 0.000265 | | |
| Total | 52 | 0.181771 | | | | |

The model created from the analysis is provided in Table 28.

Table 28 – Model of Internal Bond Results

| Term | Coefficient | P Value |
|---|---|---|
| Constant | 0.066302 | 0.168 |
| Concentration | -0.014848 | 0.073 |
| Particle Size | 0.000189 | 0.326 |
| **Concentration^2** | 0.001256 | 0.002 |
| **Particle Size^2** | 0.000001 | 0.007 |
| **Concentration*Particle Size** | -0.000055 | 0 |
| R-Squared = 0.7175 | | |

The model's coefficients showed that of the significant variables, the squared concentration interaction had the highest effect. The contour plot of the model is depicted in Figure 37. This model shows that the superior formulation of DDGS filler would be 5 wt. % - 500 µm.

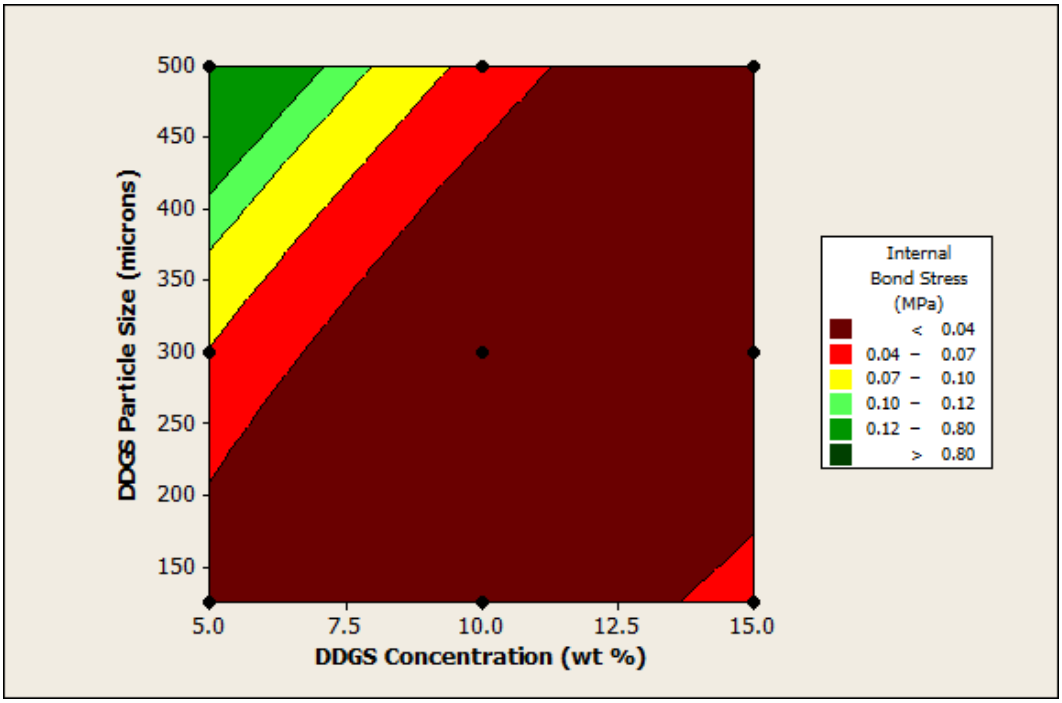


Figure 37 – Contour Plot of Internal Bond Stress

### 5.2.6 – Hardness Testing

The hardness tests showed that there was a large variation of hardness values among the samples of the sample blend. In order to reduce the variation, twenty hardness tests were performed for each blend.

As observed in Figure 38, the variation of the hardness data was considerable, and increasing the sample size did not reduce the variability. The spread of the data fell mostly within the range of the control sample with slight variation to the mean hardness values. The variation of hardness was caused by the randomness of the samples tested. The edges of the boards were found to be much softer than the center of the boards. This effect is likely attributed to the processing methods.

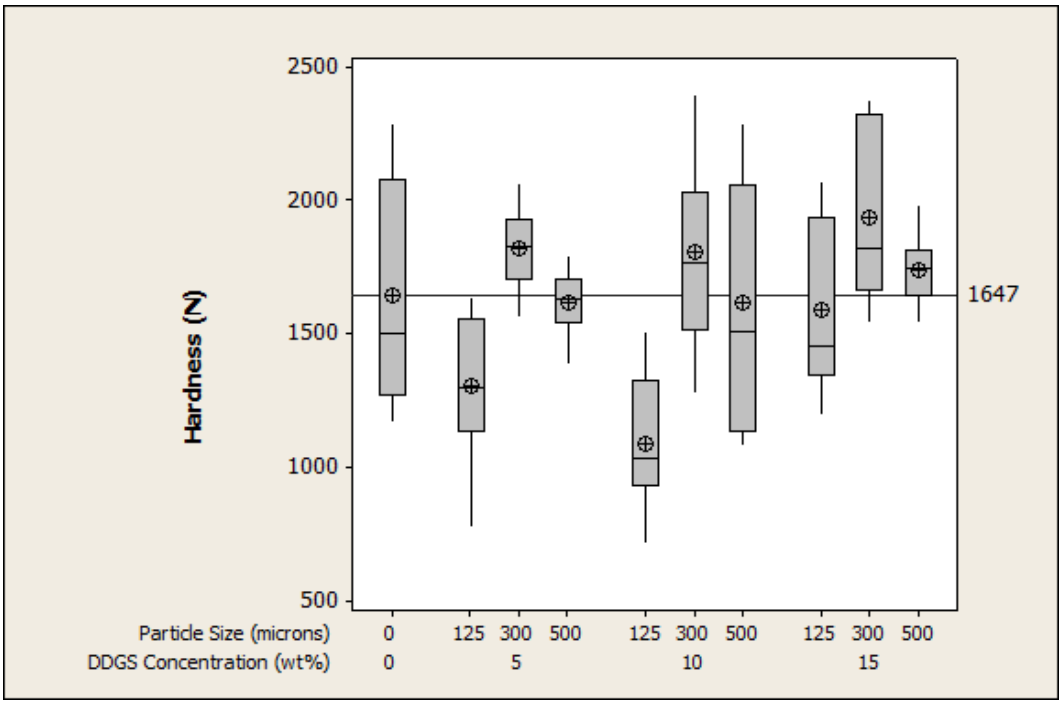


Figure 38 – Boxplot of Hardness Test Data

The Student's t test comparison of means (Table 29) showed that only the 5 wt. % and 10 wt. % at 125 µm were statistically different from the control sample. Both of these samples showed statistically lower means than the control sample.

Table 29 – Two-Way T Test of Hardness Tests

| Sample Concentration | Sample Particle Size | t - value | P - value |
|---|---|---|---|
| 0 | 0 | 0 | 1 |
| 5 | 125 | 2.38 | 0.028 |
| 5 | 300 | -1.43 | 0.173 |
| 5 | 500 | 0.21 | 0.834 |
| 10 | 125 | 4.13 | 0.001 |
| 10 | 300 | -1.05 | 0.307 |
| 10 | 500 | 0.15 | 0.884 |
| 15 | 125 | 0.36 | 0.723 |
| 15 | 300 | -1.83 | 0.084 |
| 15 | 500 | -0.78 | 0.448 |

The ANOVA test (Table 30) showed that both the particle size and concentration as well as the squared interactions of the particle size and concentration were significant.

Table 30 – ANOVA of Hardness Tests

| | DF | Seq SS | Adj SS | Adj MS | F | P |
|---|---|---|---|---|---|---|
| Regression | 5 | 5772605 | 5772605 | 1154521 | 13.54 | 0 |
| Linear | 2 | 2160212 | 4097964 | 2048982 | 24.03 | 0 |
| DDGS Concentration | 1 | 401105 | 343231 | 343231 | 4.03 | 0.048 |
| Particle Size | 1 | 1759107 | 3520127 | 3520127 | 41.28 | 0 |
| Square | 2 | 3546030 | 3541026 | 1770513 | 20.76 | 0 |
| Concentration^2 | 1 | 557432 | 630377 | 630377 | 7.39 | 0.008 |
| Particle size^2 | 1 | 2988599 | 2978273 | 2978273 | 34.93 | 0 |
| Interaction | 1 | 66362 | 66362 | 66362 | 0.78 | 0.38 |
| Concentration*Particle Size | 1 | 66362 | 66362 | 66362 | 0.78 | 0.38 |
| Residual error | 86 | 7333274 | 7333274 | 85271 | | |
| Lack of Fit | 3 | 457971 | 457971 | 152657 | 1.84 | 0.146 |
| Pure Error | 83 | 6875303 | 6875303 | 82835 | | |
| Total | 91 | 13105879 | | | | |

The model created from the ANOVA analysis (Table 31) identified that the concentration was the most influential significant variable, and a smaller concentration is preferred.

Table 31 – Model of Hardness Results

| Term | Coefficient | P Value |
|---|---|---|
| Constant | 792.4 | 0.012 |
| **Concentration** | **-106.5** | **0.048** |
| **Particle Size** | **8.152** | **0.000** |
| **Concentration^2** | **6.865** | **0.008** |
| **Particle Size^2** | **-0.011** | **0.000** |
| Concentration*Particle Size | -0.044 | 0.380 |
| R-Squared = 0.441 | | |

The contour plot shown in Figure 39, predicts that an increase of hardness can be achieved with the incorporation of DDGS. While the model predicts an increased hardness, the different tests' means are statistically equivalent. Of the DDGS blends, the model

predicts that 5 wt. % and 15 wt. % at 300 µm would produce the highest hardness properties.

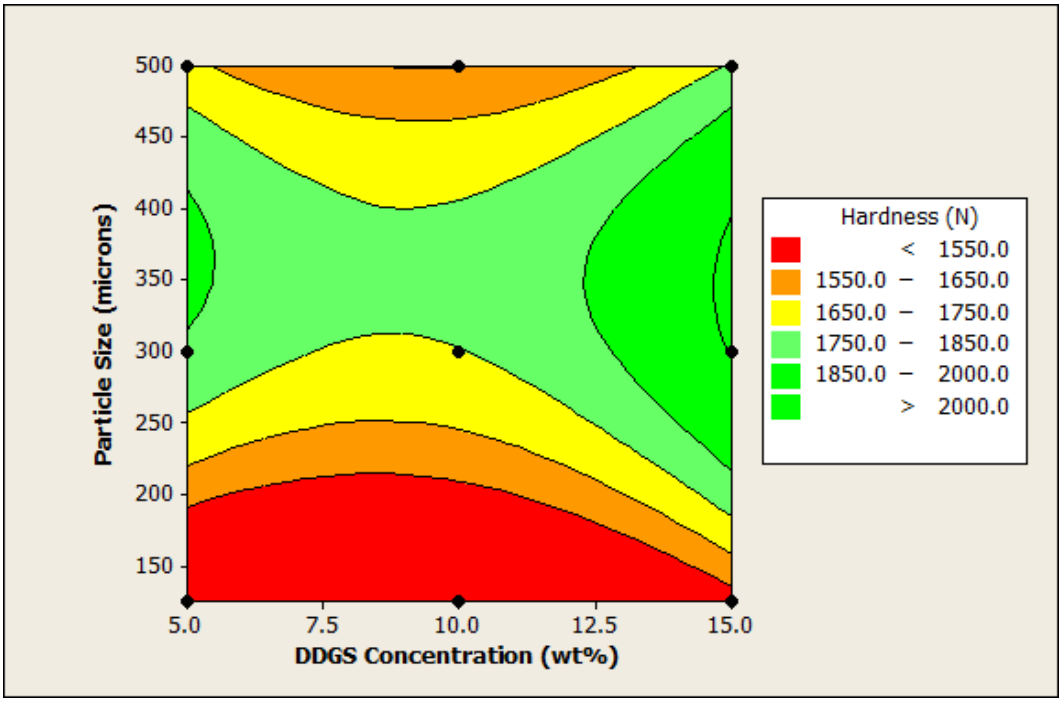


Figure 39 – Contour Plot of Hardness Test

### 5.2.7 – Screw Withdrawal Tests

Ten samples per batch were cut at random from the tested flexural samples and used for the screw withdrawal tests. These results are provided in Figure 40. The results showed a generally decreasing force value with added DDGS filler except for the 5 wt. % - 300 µm case.

From the t test, only the 10 wt. % and 15 wt. % samples at 125 µm were statistically different from the control sample (
Table 32). These two batches had statistically lower means than the control sample. The rest of the batches were statistically equivalent with 95% confidence.

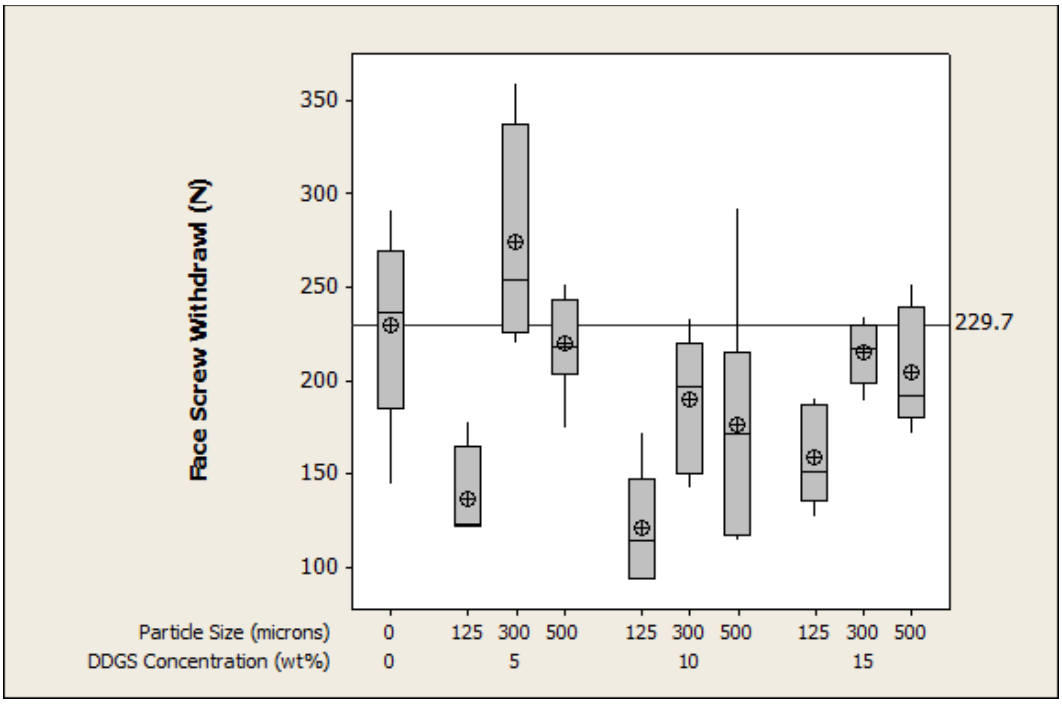


Figure 40 – Boxplot of Screw Withdrawal Results

Table 32 – Two-Way T Test of Means for Screw Withdrawal

| Sample Concentration | Sample Particle Size | t - value | P - value |
|---|---|---|---|
| 0 | 0 | 0 | 1 |
| 5 | 125 | 3.36 | 1.015 |
| 5 | 300 | -1.34 | 0.218 |
| 5 | 500 | 0.38 | 0.721 |
| 10 | 125 | 4.01 | 0.007 |
| 10 | 300 | 1.41 | 0.208 |
| 10 | 500 | 1.49 | 0.174 |
| 15 | 125 | 2.63 | 0.047 |
| 15 | 300 | 0.59 | 0.589 |
| 15 | 500 | 0.93 | 0.388 |

The ANOVA analysis showed that the concentration and particle size linear and squared interactions were significant variables (Table 33).

Table 33 – ANOVA of Screw Withdrawal Tests

| | DF | Seq SS | Adj SS | Adj MS | F | P |
|---|---|---|---|---|---|---|
| Regression | 5 | 88926 | 88926.1 | 17785.2 | 10.71 | 0 |
| Linear | 2 | 30269 | 70899 | 35449.5 | 21.35 | 0 |
| DDGS Concentration | 1 | 5383 | 16026 | 16026 | 9.65 | 0.003 |
| Particle Size | 1 | 24887 | 44127.3 | 44127.3 | 26.57 | 0 |
| Square | 2 | 57686 | 57881.7 | 28940.9 | 17.43 | 0 |
| Concentration^2 | 1 | 19778 | 18695.1 | 18695.1 | 11.26 | 0.002 |
| Particle size^2 | 1 | 37909 | 38280.5 | 38280.5 | 23.05 | 0 |
| Interaction | 1 | 971 | 970.6 | 970.6 | 0.58 | 0.449 |
| Concentration*Particle Size | 1 | 971 | 970.6 | 970.6 | 0.58 | 0.449 |
| Residual error | 44 | 73072 | 73071.7 | 1660.7 | | |
| Lack of Fit | 3 | 9001 | 9001.2 | 3000.4 | 1.92 | 0.141 |
| Pure Error | 41 | 64070 | 64070.5 | 1562.7 | | |
| Total | 49 | 161998 | | | | |

The model (Table 34), with an R squared of 0.549, showed that the linear concentration had the highest influence of the significant variables, and a smaller concentration is beneficial.

Table 34 – Model for Screw Withdrawal

| Term | Coefficient | P Value |
|---|---|---|
| Constant | 147 | 0.025 |
| **Concentration** | **-31.97** | **0.003** |
| **Particle Size** | **1.281** | **0.000** |
| **Concentration^2** | **1.615** | **0.002** |
| **Particle Size^2** | **-0.002** | **0.000** |
| Concentration*Particle Size | -0.007 | 0.449 |
| R-Squared = 0.549 | | |

The contour plot from the model (Figure 41) predicts that the 5 wt. % DDGS at 300 µm or 500 µm would produce the highest screw withdrawal properties.

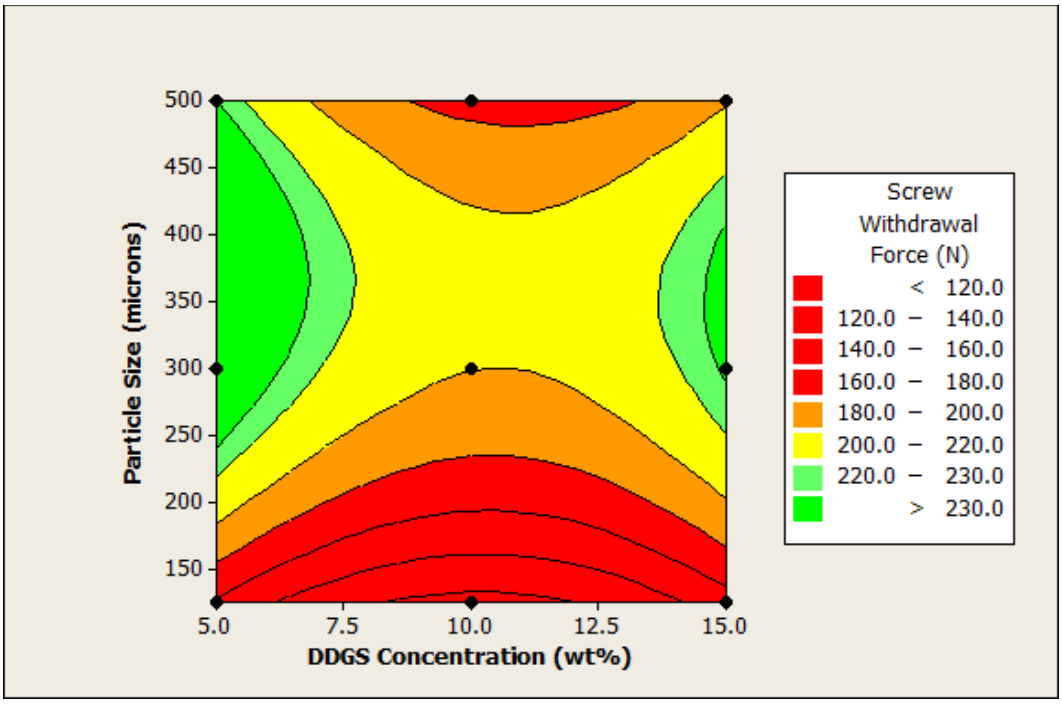


Figure 41 – Contour Plot of Screw Withdrawal Model

### 5.2.8 – Discussion of Mechanical and Physical Testing

Through the mechanical and physical testing, the ideal concentration of DDGS filler was found to be 5 wt. % and the ideal particle size of 500 µm or the unprocessed DDGS followed by the 300 µm particles. The results also show that the 125 µm particle sizes were detrimental to the properties across the board.

It is believed that the unprocessed DDGS particles are preferred due to the similarity of the unprocessed DDGS and the wood fiber's particle sizes. These particle sizes are depicted in Table 35. These two fibers have a similar particle size but that also affects the distribution of the particles within the particleboards.

Table 35 – Particle Size Comparison

| U.S. Standard Sieve and Micron Equivalent | Wood Fiber | Unprocessed DDGS |
|---|---|---|
| 20 Mesh (850 µm) | 0 – 5 % | 13.00 % |
| 40 Mesh (425 µm) | 40 – 80 % | 51.00 % |
| 60 Mesh (250 µm) | 15 – 55 % | 20 % |
| 80 Mesh (177 µm) | - | 11 % |
| Pan | < 10 % | 5 % |

It was observed during the processing that the small particles did not distribute through the wood fibers. The 125 µm particles clumped together and migrated toward the exterior surfaces of the cement mixer. The 300 and 500 µm particles were similar enough to the wood fibers that they distributed throughout the wood fibers and did not clump.

The aforementioned results showed that the 125 µm filler was detrimental to the mechanical and physical properties. Besides the difficulties that arouse during processing, the surface areas of the particles have been changed dramatically. With the reduction of particle size, the effective surface area of the particles increased. The decrease of the properties could be contributed to a poor distribution of the resin through the exposed surfaces of the particles. It may be that with the increase of the surface area needs an increase of the resin content to maintain properties.

Also noticed through this research is the deviation among the mechanical tests. The samples for testing were chosen randomly throughout the samples. Within each panel, the density varied depending upon the position of the sample. The edges of the sample were less dense than the center of the sample. This phenomenon can be observed in Figure 42 and was confirmed in the SEM images in section 5.3. Figure 42 shows the density change along the length of the linear expansion test specimens. Eight 38 mm wide samples were cut and the density was computed. In the figure the density is reported based upon the center of each sample.

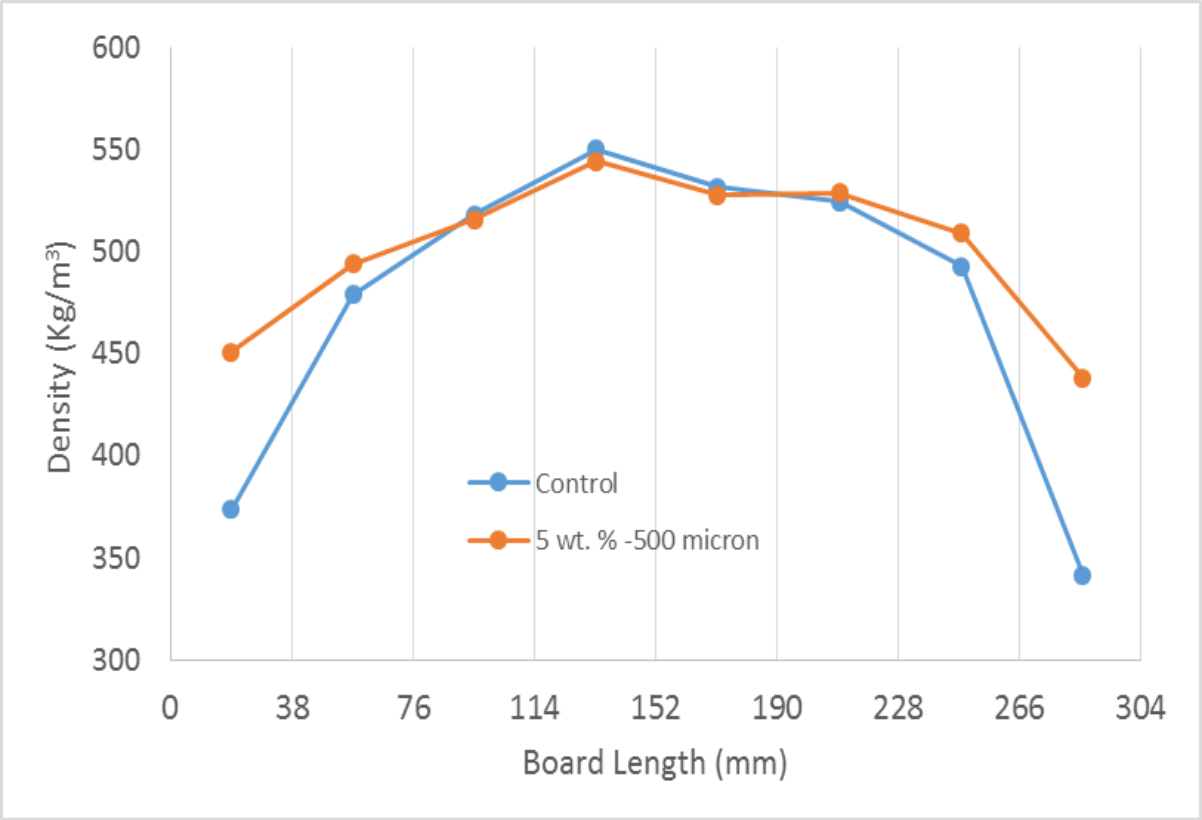


Figure 42 – Density Change across Panel Length

The results from this testing do not meet the industrial standards provided in Table 2. Table 36 compares the control sample and the 5 wt. % - 500 µm samples to the industrial standards. It shows that the control boards produced did not meet any of the industrial standards. The optimal DDGS blend also did meet the ANSI standard for the linear expansion and the internal bond strength but failed with the other properties. The fact that the industrial properties were not met is not an issue since this study compared to the control boards produced with a similar process.

Table 36 – Comparison to ANSI Standard

| Property | | ANSI Standard | Control Board | 5 wt % - 500 µm |
|---|---|---|---|---|
| Modulus of Rupture | (N/mm2) | 2.8 | 2 | 2.4 |
| Elastic Modulus | (N/mm2) | 500 | 227 | 370 |
| Internal Bond Strength | (N/mm2) | 0.1 | 0.07 | 0.2 |
| Screw Withdrawal | (N) | 360 | 229 | 219 |
| Linear Expansion | (% Change) | 0.4 | 0.0015 | 0.002 |

Further work would benefit from a trial on an industrial process that is already producing boards meeting the ANSI property standards.

## 5.3 – Scanning Electron Microscopy Results

Scanning electron microscopy (SEM) was used to investigate the distribution of DDGS particles and the packing of the fibers. Seven samples were searched to obtain clear images. Four samples from the fracture surface of the control board and 15 wt. % DDGS blends were used. The edges of the flexural sample of the 15 wt. % DDGS blends were also imaged.

In Figure 43, the orientation of the wood fibers is easy to see. With the high-compression forces during processing, the fibers have aligned themselves perpendicular to the direction of the compressive load. The DDGS particles are harder to see in Figure 43 b through d. The particles tended to settle within the voids caused by the structure. In b and c, the DDGS particles are easier to identify due to the smaller particle size and more uniform shape.

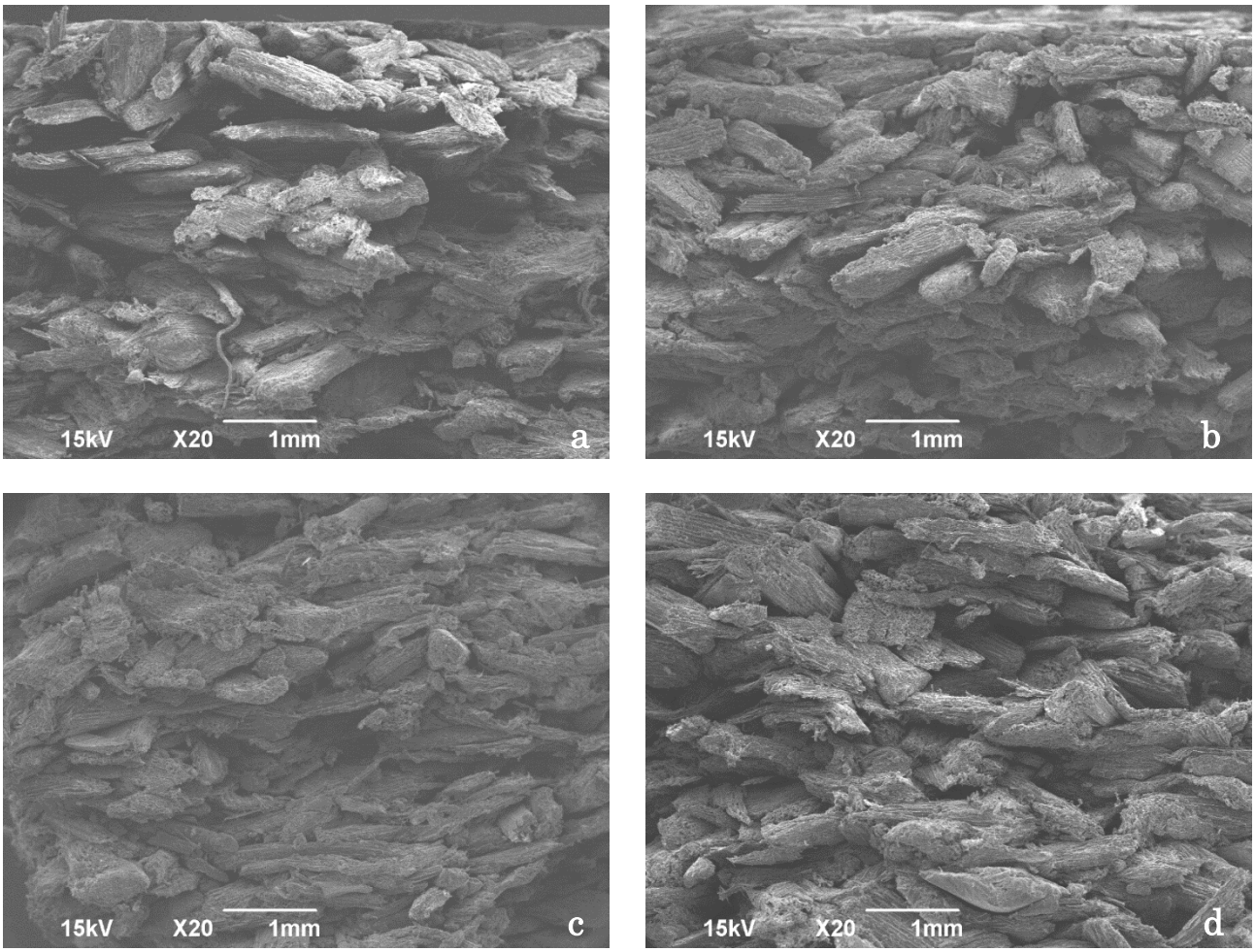


Figure 43 – SEM Image from Flexural Fracture Surface 20x Magnification
a – Control Sample, b – 125 µm, c – 300 µm, d – 500 µm

The fracture pattern observed is similar to a transgranular type fracture where the failure occurs in the binder between particles rather than in the particles themselves. This is clearly seen in Figure 44 with improved magnification. In these images, it is clearly seen that the fracture did not cause fracture in the particles. Unfortunately, additional magnification was not possible to observe the resin coating on the surface of the particles due to sample charging.

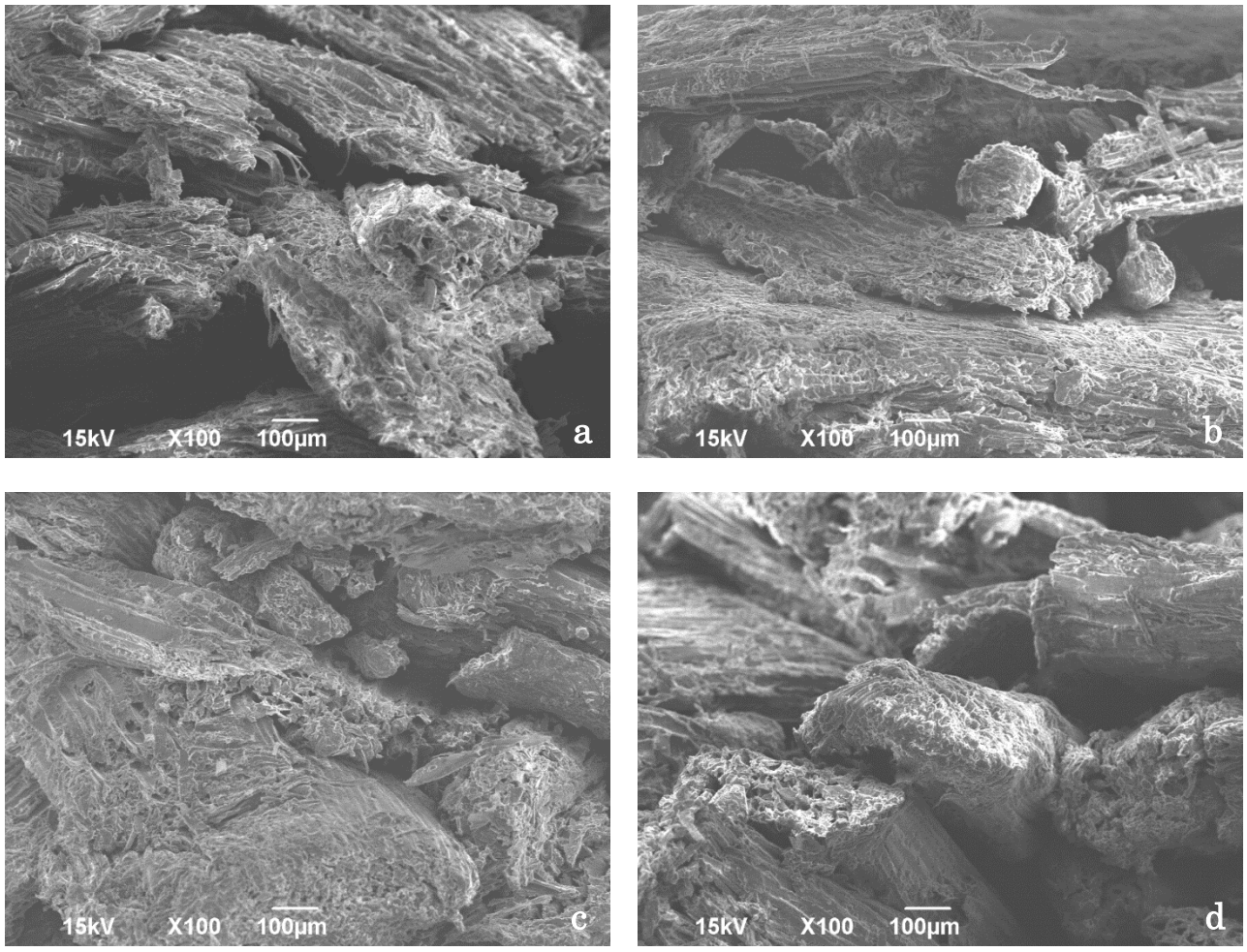


Figure 44 – SEM Images Flexural Fracture Surface 100x Magnification
a – Control Sample, b – 125 µm, c – 300 µm, d – 500 µm

Unlike the fracture surfaces at the center of the boards, the edges of the samples showed a more random distribution of the wood particles. This random orientation decreased the packing of the particles and thus also the density of the edges of the boards. The DDGS particles followed the same distribution pattern in the edge as the center samples.

The differences in fiber orientation between the edge of the board and the center of the board produced differences in the density of the samples. These differences can easily cause the spread of the data observed in the mechanical testing, especially the screw

withdrawal and hardness tests. This distribution of density is unfortunately uncontrollable but was substantially reduced in the current processing methods.

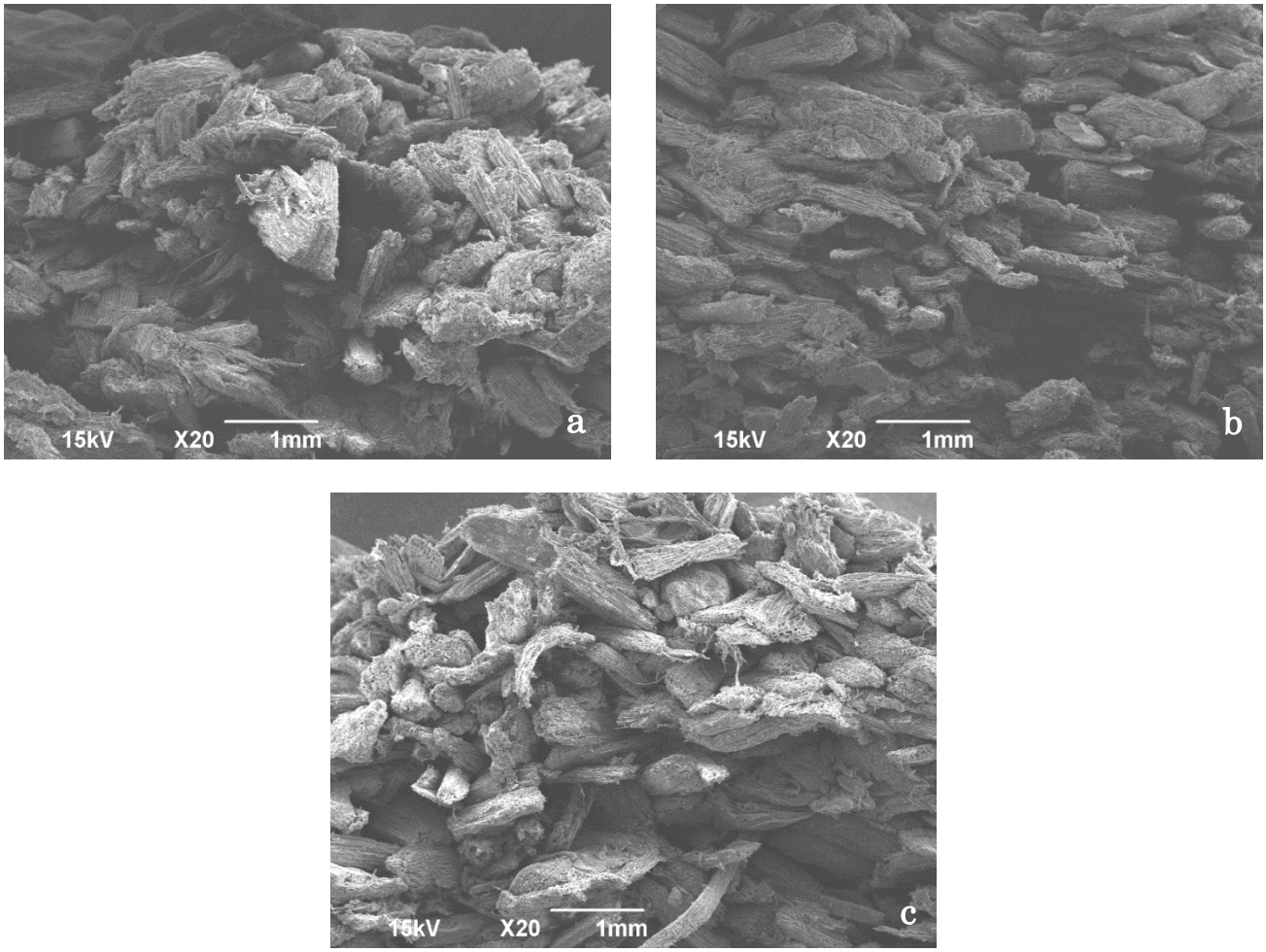


Figure 45 – SEM Image of Edge of Samples 20x magnification

a –125 µm, b – 300 µm, c – 500 µm

## 5.4 – Economic Analysis

This research showed that the addition of DDGS produced increases in the mechanical properties of the flexural modulus, elastic modulus, and internal bond test. The addition of DDGS has also been shown to improve the water absorption resistance of the samples. In order to quantify the added benefit of incorporating DDGS filler into the particleboards, a simple economic analysis was performed. This analysis was performed

using costs of materials from this experiment and will vary based upon the order size. The component costs are listed in Table 37.

Table 37 – Experiment's Component Cost

| Component | Cost per Pound ($/lb) |
|---|---|
| MUF Resin | 0.25 |
| Paraffin Wax | 2.57 |
| Wood Fiber | 0.25 |
| DDGS | 0.09 |

It is clear that the cost of the paraffin wax is the most expensive component and if the DDGS fats could be substituted for the wax it would greatly reduce the cost of the boards. Assuming a low density particleboard, the cost of materials per square foot of the control board is calculated.

Table 38 – Control Panel Costs

| | Blend | Component Cost |
|---|---|---|
| MUF Resin | 0.1 | $ 0.04 |
| Paraffin Wax | 0.1 | $ 0.40 |
| Wood Fiber | 0.8 | $ 0.31 |
| Total Cost $/(ft$^2$) | | 0.74 |
| Total Cost $/(m$^2$) | | 8.00 |

The addition of DDGS at the recommended concentration of 5 wt. % reduces the cost per square meter of particleboard by $0.13 as seen in Table 39. If the cost savings are preferred over the increase of mechanical properties, the DDGS can be substituted for MUF resin and the paraffin wax. Assuming that the MUF resin and paraffin wax can be reduced to 8 wt. % and 5 wt. % — while maintaining statistical equivalence to the control board — and replaced with DDGS, the total savings per square meter of board would be $ 2.24.

Table 39 – Preferred DDGS Concentration Costs

| | Blend | Component Cost |
|---|---|---|
| MUF Resin | 0.1 | $ 0.04 |
| Paraffin Wax | 0.1 | $ 0.40 |
| Wood Fiber | 0.75 | $ 0.29 |
| DDGS | 0.05 | $ 0.01 |
| Total Cost $/(ft$^2$) | | 0.73 |
| Total Cost $/(m$^2$) | | 7.87 |

Table 40 – Savings from Substitution of DDGS for Resin and Wax

| | Blend | Component Cost |
|---|---|---|
| MUF Resin | 0.08 | $ 0.03 |
| Paraffin Wax | 0.05 | $ 0.20 |
| Wood Fiber | 0.75 | $ 0.29 |
| DDGS | 0.12 | $ 0.02 |
| Total Cost $/(ft$^2$) | | 0.53 |
| Total Cost $/(m$^2$) | | 5.76 |

In 2012, the total particleboard production exceeded 3.2 billion square feet [1]. If the use of DDGS was implemented in all the boards produced at 5 wt. %, the maximum savings could amount to $32 Million assuming $0.01 savings per square foot of particleboard. This analysis shows that the use of DDGS in particleboards can reduce the cost of the particleboards. The extent of the savings is hypothesized could potentially be $ 2.24 per square meter of board but more research needs to be completed at differing concentrations of resin and wax to verify the assumption of the equivalency of properties.

# CHAPTER 6 – CONCLUSIONS AND RECOMMENDATIONS

This study investigated the effect of the addition of dried distiller's grains with solubles (DDGS) as a functional filler in wood particleboards. The chemical and mechanical properties were tested and analyzed using statistical methods. Four hypotheses were fundamental to the research. These hypotheses were as follows:

H1: The protein of the DDGS can be decoupled via heat and subsequently fully bond to the MUF resin.

H2: The decrease of particle size of the DDGS filler will improve the mechanical properties.

H3: Higher concentrations of DDGS will not significantly influence the mechanical performance of the particleboards.

H4: The residual fat in DDGS will decrease the linear expansion and water absorption of the particleboards.

H1 Conclusion: The DDGS was analyzed via TGA and DSC tests. The TGA test showed that the degradation temperature of DDGS was between 250 ˚C and 300 ˚C. This test also showed that partial degradation occurred up to 200 ˚C. The DSC test studied the degradation of DDGS and the bonding of the MUF resin. This test showed that the DDGS can decouple and subsequently bond to the MUF resin. These findings fail to reject H1 by demonstrating that DDGS can be decoupled and subsequently bound to the MUF resin.

H2 Conclusion: Mechanical testing studied the effects of the DDGS particle size on the mechanical properties of the particleboards. The flexural properties and the internal bond strength showed significant improvement with the addition of 500 µm DDGS filler, whereas the hardness and the screw withdrawal strength remained statistically equivalent

to the control sample. In all tests, the decrease of particle size did not improve the mechanical properties of the particleboards. The various particle sizes of DDGS produced equivalent degradation curves from the TGA and DSC tests. Chemical analysis also showed that there were not any large differences among the chemical compositions of the particle sizes. This seems to suggest that the loss of mechanical properties using the 125 µm fillers are not attributed to the processing method. The SEM images did show that the distribution of the DDGS was inconsistent. Compounding upon the inhomogeneous nature of particleboards, the 125 µm DDGS particles were poorly distributed through the samples causing no additional benefit of the micronized particles.

The models predicted that the best formulation of DDGS filler was 5 wt. % DDGS at 500 µm. The results also suggested that 5 wt. % DDGS at 300 µm could also be an option. Because mechanical testing showed that the micronization of DDGS filler did not globally improve the mechanical properties of the panels, H2 is rejected.

H3 Conclusion: The increase of DDGS concentration did not significantly influence the mechanical properties of the particleboards for the mechanical tests. Interestingly, at lower concentrations of DDGS filler, the mechanical properties improved whereas at higher concentrations, the mechanical properties remained statistically equivalent to the control sample. These results fail to reject H3 because, as the hypothesis suggests, higher concentrations did not influence mechanical properties.

H4 Conclusion: The linear expansion and water absorption tests were performed. The results showed that the addition of DDGS filler did not produce a significant change in the linear expansion properties. The water absorption test showed that after 24 hours, the volume change of all DDGS samples was lower than the control sample. Of these samples, the samples which had the particle size of 500 µm were significantly smaller than the

control sample. These results fail to reject H4 because the tests showed that the addition of DDGS can improve the moisture resilience of particleboards.

In summary, this study showed that the incorporation of DDGS into particleboards can improve some, but not all, of the mechanical properties as well as the moisture resilience. The formulation of DDGS that improved the mechanical and physical properties of the boards possessed a concentration of 5 wt. % and particle size of 500 µm.

The use of DDGS in particleboards can decrease the demand for logged wood for construction materials. The additional benefits of DDGS are that it is produced from an annual crop, and the increasing demand for ethanol suggests that the supply of DDGS will not diminish in the future.

This thesis simply scratches the surface of the research that can be conducted into DDGS- filled building products. Additional research into DDGS-filled particleboards could investigate the effect of DDGS using different resin systems such as PF's and MDI's. Future research should also strive to optimize the curing time for the panels. Finally, the commercialization of DDGS filled particleboards should be investigated and an industrial trial should be performed adhering to industrial standards.

# REFERENCES/ WORKS CITED


[1] A. Wood Council and C. Wood Council, "Particleboard Environmental Product Declaration," 2013.

[2] Forest Products Laboratory, "Wood Handbook: Wood as an Engineering Material," U.S. Department of Agriculture, 2010.

[3] E. Sjostrom, *Wood Chemistry. Fundamentals and Applications.*, 2nd ed. San Diego: Academic Press, 1993.

[4] "No Title." [Online]. Available: http://www.lbl.gov/Publications/YOS/assets/img/biofuels_evolution.jpg.

[5] R. Hatfield and W. Vermerris, "Lignin formation in plants. The dilemma of linkage specificity.," *Plant Physiol.*, vol. 126, no. 4, pp. 1351–1357, 2001.

[6] ASTM International, "ASTM D1554 - 10: Standard Terminology Relating to Wood-Base Fiber and Particle Panel Materials 1," vol. 3. pp. 31–34, 2013.

[7] T. M. Maloney, *Modern particleboard & dry-process fiberboard manufacturing*. San Francisco, CA: Miller Freeman Publications, 1977.

[8] K. Cabinets, D. Core, M. H. Decking, S. Treads, F. Underlayment, R. Furniture, and S. Fixtures, "Particleboard."

[9] S. Oswalt, M. Thompson, and W. B. Smith, "U.S. Forest Resource Facts and Historical Trends," 2010.

[10] Food and Agriculture Organization of the United Nations, "The North American Forest Sector Outlook Study 2006 - 2030," 2006.

[11] "Particleboard and medium-density fiberboard: Choose Green Report," 2001.

[12] A. L. Lambuth and I. Introduction, "Protein Adhesives for Wood," in *Handbook of Adhesive Technology*, Taylor & Francis Group, 2003, pp. 457–478.

[13] C. L. Pearson, "Animal Glues and Adhesives," in *Handbook of Adhesive Technology*, Taylor & Francis, 2003, pp. 479–494.

[14] P. Argos, K. Pedersen, M. D. Marks, and B. a Larkins, "A structural model for maize zein proteins.," *J. Biol. Chem.*, vol. 257, no. 17, pp. 9984–90, Sep. 1982.

[15] K. S. Liu and K. A. Rosentrater, *Distillers Grains: Production, Properties, and Utilization*. Taylor & Francis, 2011.

[16] T. Capehart, E. Allen, and J. K. Bond, “Feed Outlook: November 2013,” 2013.

[17] R. fuels A. RFA, “Battling for the Barrel 2013 Ethanol Industry Outlook,” 2013.

[18] T. Tabarsa, S. Jahanshahi, and A. Ashori, “Mechanical and physical properties of wheat straw boards bonded with a tannin modified phenol–formaldehyde adhesive,” *Compos. Part B*, vol. 42, no. 2, pp. 176–180, Mar. 2011.

[19] J. Xu, R. Widyorini, H. Yamauchi, and S. Kawai, “Development of binderless fiberboard from kenaf core,” *J. Wood Sci.*, vol. 52, no. 3, pp. 236–243, Jun. 2006.

[20] S. Khosravi, F. Khabbaz, P. Nordqvist, and M. Johansson, “Protein-based adhesives for particleboards,” *Ind. Crops Prod.*, vol. 32, no. 3, pp. 275–283, Nov. 2010.

[21] M. Ando and M. Sato, “Manufacture of plywood bonded with kenaf core powder,” *J. Wood Sci.*, vol. 55, no. 4, pp. 283–288, Mar. 2009.

[22] R. Widyorini, J. Xu, K. Umemura, and S. Kawai, “Manufacture and properties of binderless particleboard from bagasse I: effects of raw material type, storage methods, and manufacturing process,” *J. Wood Sci.*, vol. 51, no. 6, pp. 648–654, Dec. 2005.

[23] B. Sarı, G. Nemli, N. Ayrilmis, M. Baharoğlu, and S. Bardak, “The Influences of Drying Temperature of Wood Particles on the Quality Properties of Particleboard Composite,” *Dry. Technol.*, vol. 31, no. 1, pp. 17–23, Jan. 2013.

[24] A. W. Christiansen, “How Overdrying Wood Reduces Its Bonding to Phenol-Formaldehyde Adhesives,” *WOOD FIBER Sci.*, vol. 22, no. 4, pp. 441–459, Oct. 1990.

[25] B. Lauke, X.-Q. Feng, Y.-W. Mai, and S.-Y. Fu, “Effects of particle size, particle/matrix interface adhesion and particle loading on mechanical properties of particulate–polymer composites,” *Compos. Part B Eng.*, vol. 39, no. 6, pp. 933–961, Sep. 2008.

[26] J. Cho, M. S. Joshi, and C. T. Sun, “Effect of inclusion size on mechanical properties of polymeric composites with micro and nano particles,” *Compos. Sci. Technol.*, vol. 66, no. 13, pp. 1941–1952, Oct. 2006.

[27] E. Arzt, “Size Effects in Materials Due to Microstructural and Dimensional Constraints : A Comparitive Review,” *Acta Mater.*, vol. 46, no. 16, pp. 5611–5626, 1998.

[28] J. L. Julson, G. Subbarao, D. D. Stokke, H. H. Gieselman, and K. Muthukumarappan, “Mechanical properties of biorenewable fiber/plastic composites,” *J. Appl. Polym. Sci.*, vol. 93, no. 5, pp. 2484–2493, Sep. 2004.

[29] H. N. Cheng, M. K. Dowd, and Z. He, “Investigation of modified cottonseed protein adhesives for wood composites,” *Ind. Crops Prod.*, vol. 46, pp. 399–403, Apr. 2013.

[30] A. Moubarik, A. Allal, A. Pizzi, F. Charrier, and B. Charrier, "Characterization of a formaldehyde-free cornstarch-tannin wood adhesive for interior plywood," *Eur. J. Wood Wood Prod.*, vol. 68, no. 4, pp. 427–433, Dec. 2009.

[31] A. Moubarik, A. Pizzi, A. Allal, F. Charrier, A. Khoukh, and B. Charrier, "Cornstarch-mimosa tannin-urea formaldehyde resins as adhesives in the particleboard production," *Starch - Stärke*, vol. 62, no. 3–4, pp. 131–138, Apr. 2010.

[32] M. Ando and M. Sato, "Evaluation of the self-bonding ability of sugi and application of sugi powder as a binder for plywood," *J. Wood Sci.*, vol. 56, no. 3, pp. 194–200, Mar. 2010.

[33] R. Alexander, "Industrial uses of dry-milled corn products," in *Industrial uses of Cereals*, 1973, pp. 303–15.

[34] R. Alexander and R. Krueger, "Art of Manufacturing compression molded particle board with nitrogenous modified amylaceous binder.," 3,983,084, 1973.

[35] S. Kim, J. Xu, and S. Liu, "Production of biopolymer composites by particle bonding," *Compos. Part A Appl. Sci. Manuf.*, vol. 41, no. 1, pp. 146–153, Jan. 2010.

[36] M. D. H. Beg, K. L. Pickering, and S. J. Weal, "Corn gluten meal as a biodegradable matrix material in wood fibre reinforced composites," *Mater. Sci. Eng. A*, vol. 412, no. 1–2, pp. 7–11, Dec. 2005.

[37] I. Yang, M. Kuo, D. J. Myers, and A. Pu, "Comparison of protein-based adhesive resins for wood composites," *J. Wood Sci.*, vol. 52, no. 6, pp. 503–508, Dec. 2006.

[38] P. Nordqvist, N. Nordgren, F. Khabbaz, and E. Malmström, "Plant proteins as wood adhesives: Bonding performance at the macro- and nanoscale," *Ind. Crops Prod.*, vol. 44, pp. 246–252, Jan. 2013.

[39] A. P. Abbott, J. Palazuela Conde, S. J. Davis, and W. R. Wise, "Starch as a replacement for urea-formaldehyde in medium density fibreboard," *Green Chem.*, vol. 14, no. 11, p. 3067, 2012.

[40] S. Nonaka, K. Umemura, and S. Kawai, "Characterization of bagasse binderless particleboard manufactured in high-temperature range," *J. Wood Sci.*, vol. 59, no. 1, pp. 50–56, Oct. 2012.

[41] COST Action E20, "Wood material science research program. Wood fibre cell wall structure.," 2003.

[42] N. Nikvash, R. Kraft, A. Kharazipour, and M. Euring, "Comparative properties of bagasse, canola and hemp particle boards," *Eur. J. Wood Wood Prod.*, vol. 68, no. 3, pp. 323–327, Jul. 2010.

[43] K. A. Rosentrater, "Some Physical Properties of Distillers Dried Grains with Solubles," *Appl. Eng. Agric.*, vol. 22, no. 4, pp. 589–595, 2006.

[44] K. Liu, "Particle size distribution of distillers dried grains with solubles (DDGS) and relationships to compositional and color properties.," *Bioresour. Technol.*, vol. 99, no. 17, pp. 8421–8, Nov. 2008.

[45] R. Bhadra, K. A. Rosentrater, and K. Muthukumarappan, "Cross-Sectional Staining and Surface Properties of DDGS Particles and Their Influence on Flowability," *Cereal Chem.*, vol. 86, no. 4, pp. 410–420, 2009.

[46] B. Tisserat, L. Reifschneider, and V. L. Finkenstadt, "Mechanical and Thermal Properties of High Density Polyethylene – Dried Distillers Grains with Solubles Composites," *Bioresources*, vol. 8, no. 1, pp. 59–75, 2013.

[47] R. a. Tatara, K. a. Rosentrater, and S. Suraparaju, "Design properties for molded, corn-based DDGS-filled phenolic resin," *Ind. Crops Prod.*, vol. 29, no. 1, pp. 9–15, Jan. 2009.

[48] S. Suraparaju, K. a. Rosentrater, and R. a. Tatara, "Compression Molding of Phenolic Resin and Corn-based DDGS Blends," *J. Polym. Environ.*, vol. 15, no. 2, pp. 89–95, Apr. 2007.

[49] V. Cheesbrough, K. a. Rosentrater, and J. Visser, "Properties of Distillers Grains Composites: A Preliminary Investigation," *J. Polym. Environ.*, vol. 16, no. 1, pp. 40–50, Feb. 2008.

[50] D. M. Levine, P. P. Ramsey, and R. K. Smidt, *Applied Statistics for Engineers and Scientists: Using Microsoft Excel and Minitab*. Prentice Hall, 2001.

[51] P. C. . Bergman and A. R. Boersma, "Torrefaction for biomass co-firing in existing coal-fired power stations," 2005.